

Final Summer 2000

Development of a Bank Reversal Control Law for a Martian Aerocapture Guidance Algorithm

By

Justin Kyle Strickland

B.S.A.E May 1998, The University of Kansas

A Thesis submitted to

The Faculty of

The School of Engineering and Applied Science
of the George Washington University in partial satisfaction
of the requirements for the degree of Master of Science

August 2000

Thesis directed by

Dr. Robert H. Tolson

Professor of Engineering and Applied Sciences
The George Washington University

Abstract

A control logic is presented for use in a bank reversal guidance algorithm for aerocapture at Mars. Bank angle magnitude is used to control apoapsis altitude, and bank reversals are used to control inclination angle. Bank reversals are commanded when the inclination deviation from a reference exceeds a preset limit and the current direction would increase the deviation. A method for determining bank reversal boundaries is presented. Additionally, a guidance law is developed to determine the best bank direction (through full lift up or full lift down) for each bank reversal to maximize the periapsis altitude of the final orbit. The advantage of the maximum periapsis altitude is the lower velocity change required to circularize the orbit. Another advantage is the reduced decay rate of the resulting orbit that increases mission safety in the event that the periapsis raise maneuver cannot be immediately performed.

For application to a complete numerical simulation, an angular motion model is also developed. This model is used to simulate rigid body rotations, with finite angular rates and accelerations, without solving the rotational equations of motion. This algorithm is included in a three degree-of-freedom simulation to approximate the behavior of a six degree-of-freedom simulation.

These developments are brought together with a bank reversal guidance algorithm to create a complete aerocapture simulation. The control logic is tested for robustness and effectiveness. The results show that the control law is easily applicable to an aerocapture problem, and does increase the final periapsis altitude over other control methods.

Acknowledgments

There are many people who deserve my gratitude for helping to realize this goal. First, without my parents and their support, I would not be where I am today (in more ways than one). My friends and family have been unconditionally supportive every step of the way.

I would like to thank my advisor, Dr. Tolson, for always explaining in ten minutes how to overcome the barrier I had been working on for ten days. I owe thanks to Dick Powell for always having a clear goal in his head and orchestrating the path of my research. Scott Striepe has been my guide to POST (“he says confidently”), teaching me how to “trick” it into doing what I want, as well as my guide to a more enjoyable March Madness. John Aquirre has always been there to help with modifying and running POST, fixing UNIX problems (or rather user problems), and supplying baked goods to die for. My adventure though the Apollo algorithm would never have been completed if not for Eric Queen, who took the time to ponder the next step, after declaring “He’s baack,” each time I appeared at his desk. My research has been built upon the data provided by Michelle Munk, who should be credited with starting me in the right direction. Prasun Desai has helped me understand the workings of the JIAFS program, and with the occasional POST question. And finally, my gratitude goes out to everyone in the VAB, who have all been welcoming from the start.

Thank you all. Your help, support, and kindness have not gone unappreciated.

Table of Contents

Abstract	i
Acknowledgments	ii
Table of Contents	iii
List of Figures.....	v
List of Tables	vii
Nomenclature	viii
1 Introduction.....	1
1.1 Background of Aeroassist Maneuvers	1
1.2 Spacecraft Guidance Routines	2
1.3 Application of Guidance to Aerocapture.....	3
2 Angular Motion Simulation	5
2.1 Method Development	5
2.2 Flow of Bank Dynamics Model	8
2.3 Application to Simulation	10
3 Simulation Development	11
3.1 POST General Simulation Solutions	11
3.2 Mars Aerocapture Specific Simulation Input.....	12
4 Bank Reversal Control Logic.....	15
4.1 Aerocapture Simulation Boundary Condition Definition.....	16
4.2 Definition of Bank Reversal Boundaries	18
4.2.1 One Bank Reversal	19
4.2.2 Two Bank Reversals	20
4.2.3 Three Bank Reversals	21

5	Bank Direction Control Logic.....	23
5.1	Bank Direction Trade Study.....	23
5.2	Bank Direction Logic Development.....	26
5.2.1	Theory Development	26
5.2.2	Reversal Direction Criteria.....	28
5.2.3	Application to Simulation	29
5.2.3.1	Gauss' Variational Equations	29
5.2.3.2	Periapsis Specific Sensitivity Equation.....	30
5.2.3.3	Verification of Control Logic	33
5.2.3.4	Control Law Effectiveness	37
5.2.3.5	Disadvantages of Directly Applied Control Law	44
5.3	Application to Vehicle Controller	45
5.3.1	Final Inclination Boundary Definition.....	45
5.3.2	Application to Nominal Simulation.....	49
5.4	Application to Apollo Algorithm	51
6	Results.....	55
7	Conclusions.....	66
8	Future Work.....	68
	References.....	69
	Appendix A.....	A.1
	Appendix B.....	B.1

List of Figures

<u>Figure</u>	<u>Page</u>
Figure 2.1: Bank Dynamics Model Compared to Continuous Time Motion	6
Figure 2.2: Sample Bank Dynamic Model Test Case	10
Figure 3.1: Flow Diagram of POST 3-DOF Simulation (Reference 7)	12
Figure 3.2: Illustration of Vehicle Aerodynamic Characteristics	13
Figure 4.1: Aerodynamic Forces Acting on High L/D Vehicle	15
Figure 4.2: Diagram of General Aerocapture Trajectory	17
Figure 4.3: Single Bank Reversal Reference Trajectory	19
Figure 4.4: Double Bank Reversal Reference Trajectory	21
Figure 4.5: Triple Bank Reversal Reference Trajectory	22
Figure 5.1: Sample Bank Direction Trade Study Trajectory (Bank Through 0 deg)	24
Figure 5.2: Sample Bank Direction Trade Study Trajectory (Bank Through 180 deg)	24
Figure 5.3: Bank Reversal Direction and Location Affects on Periapsis Altitude	25
Figure 5.4: Illustration of Body Fixed Coordinate Systems	26
Figure 5.5: Periapsis Sensitivities for a Sample Trajectory	32
Figure 5.6: Lift Up Impulse Applied With a Positive Sensitivity	34
Figure 5.7: Lift Down Impulse Applied With a Negative Sensitivity	34
Figure 5.8: Lift Down Impulse Applied With a Positive Sensitivity	35
Figure 5.9: Lift Up Impulse Applied With a Negative Sensitivity	36
Figure 5.10: Effect of Full Lift Up Trajectory on Periapsis Altitude	38
Figure 5.11: Effect of Full Lift Down Trajectory on Periapsis Altitude	38
Figure 5.12: Effect of Best Case Lift Control on Periapsis Altitude	39
Figure 5.13: Effect of Worst Case Lift Control on Periapsis Altitude	40
Figure 5.14: Trajectory With Nominal Vertical Lift Component	42
Figure 5.15: Results of Control Law Example Scenarios	43
Figure 5.16: Sensitivity of Final Apoapsis to Initial Flight Path Angle	44
Figure 5.17: Single Bank Reversal Nominal Trajectory	46
Figure 5.18: Double Bank Reversal Nominal Trajectory	47
Figure 5.19: Triple Bank Reversal Nominal Trajectory	48
Figure 5.20: Nominal Trajectory With Bank Reversal Control Law	50

Figure 6.1: Full Simulation with Nominal Conditions.....	55
Figure 6.2: Full Simulation with -0.5 Degree Flight Path Angle Error	56
Figure 6.3: Full Simulation with +0.5 Degree Flight Path Angle Error	57
Figure 6.4: Full Simulation with +0.5 Degree Azimuth Angle Error	58
Figure 6.5: Full Simulation with -0.5 Degree Azimuth Angle Error	58
Figure 6.6: Full Simulation with +20 m/s Velocity Error	59
Figure 6.7: Full Simulation with -20 m/s Velocity Error	60
Figure 6.8: Full Simulation with Low Density Atmosphere	61
Figure 6.9: Full Simulation with High Density Atmosphere.....	61
Figure 6.10: Full Simulation with +10% Ballistic Coefficient Error.....	62
Figure 6.11: Full Simulation with -10% Ballistic Coefficient Error.....	63
Figure 6.12: Results of Full Simulation Test Cases.....	65
Figure A.1: Flow Chart of Bank Angle Dynamics Model	A.1
Figure A.2: Flow Chart of Bank Angle Dynamics Model (cont.)	A.2
Figure B.1: Flow Chart of Bank Reversal Control Logic	B.1

List of Tables

<u>Table</u>	<u>Page</u>
Table 3.1: Reference Mars Mission Specific Simulation Data.....	14
Table 5.1: Summary of Control Law Test Results	36
Table 5.2: Summary of Control Law Example Scenarios.....	43
Table 6.1: Summary of Full Simulation Test Cases	64

Nomenclature

<u>Symbol</u>	<u>Description</u>	<u>Units</u>
A	Aerodynamic Coefficient Reference Area	m ²
a	Orbit Semi-Major Axis	km
a _L	Unit Acceleration in the Lift Direction	m/s ²
a _r	Unit Acceleration Component in the RSW Frame	m/s ²
a _s	Unit Acceleration Component in the RSW Frame	m/s ²
a _z	Azimuth Angle	deg
\bar{a}_A	Aerodynamic Acceleration	m/s ²
\bar{a}_T	Thrust Acceleration	m/s ²
\dot{a}	Time Rate of Change of Semi-Major Axis	km/s
C _D	Coefficient of Lift	~
C _L	Coefficient of Drag	~
D	Drag Force	N
dt	Time Step Interval	sec
e	Orbit Eccentricity	~
\dot{e}	Time Rate of Change of Eccentricity	1/sec
\bar{e}	Unit Vector	~
f	Orbital True Anomaly	deg
\bar{g}	Acceleration due to Gravity	m/s ²
G	Apollo Algorithm Control Gain	~
h	Orbital Angular Momentum	km ² /sec
h	Vehicle Altitude	m
\dot{h}	Altitude Rate	m/s
h _a	Apoapsis Altitude	km
h _p	Periapsis Altitude	km
h _s	Scale Height	m
i	Inclination Angle	deg
Δi	Deviation of Inclination Angle From Reference	~
J ₂	Second Zonal Harmonic	~

JD	Julian Date	yr
K	Apollo Algorithm Overcontrol Factor	~
l_{ref}	Vehicle Reference Length	m
L	Lift Force	N
Long	Longitude	deg
Lat	Latitude	deg
m	Vehicle Mass	kg
M	Mach Number	~
p	Orbital Semi-Latus Rectum	km
r	Magnitude of Position Vector	km, m
\vec{r}	Position Vector From Center of the Planet to the Vehicle	m
$\dot{\vec{r}}$	Derivative of Position Vector with Respect to Time	m/s
r_e	Equatorial Radius of Planet	m
r_{polar}	Polar Radius of Planet	m
r_p	Periapsis Radius	km
\dot{r}_p	Time Rate of Change of Periapsis Radius	km/s
R	Average Surface Radius of Planet	m
S_{ref}	Vehicle Reference Area	m ²
Δt	Time Interval	sec
V	Velocity Magnitude	m/s
\vec{V}	Velocity in the Planet Centered Inertial Frame	m/s
$\dot{\vec{V}}$	Derivative of Velocity with Respect to Time	m/s ²
ΔV	Velocity Change	m/s
x	State Vector	~
\dot{x}	Time Derivative of the State Vector	~/sec

<u>Greek Symbol</u>	<u>Description</u>	<u>Units</u>
α	Angle of Attack	deg
β	Sideslip Angle	deg
$\delta\phi$	Bank Angle Difference	deg

ε	Orbital Energy	m^2/sec^2
$\hat{\varepsilon}$	Normalize Orbital Energy	~
γ	Flight Path Angle	deg
ϕ	Bank Angle	deg
$\Delta\phi$	Bank Angle Change	deg
$\dot{\phi}$	Bank Angle Rate	deg/sec
$\Delta\dot{\phi}$	Bank Angle Rate Change	deg/sec
$\ddot{\phi}$	Bank Angle Acceleration	deg/sec ²
$\Delta\ddot{\phi}$	Bank Angle Acceleration Change	deg/sec ²
λ_h	Altitude Influence Coefficient	1/sec ²
λ_s	Down Range Influence Coefficient	~
λ_u	Control Influence Coefficient	~
λ_v	Velocity Influence Coefficient	~
λ_γ	Flight Path Angle Influence Coefficient	m/sec
ρ	Atmospheric Density	kg/m^3
μ	Gravitational Parameter of Planet	m^3/sec^2
Ω	Rotation Rate of Planet	rad/sec

<u>Acronym</u>	<u>Description</u>
LVLH	Local Vertical Local Horizontal Coordinate System
MGS	Mars Global Surveyor
Mars-GRAM	Mars Global Reference Atmospheric Model
NASA	National Aeronautics and Space Administration
POST	Program to Optimize Simulated Trajectories
RCS	Reaction Control System
3-DOF	Three Degree-of-Freedom
6-DOF	Six Degree-of-Freedom
1- σ	One Standard Deviation in a Data Set (One-Sigma)

1 Introduction


The exploration of Mars continues to be a high priority for the scientific community, the National Aeronautics and Space Administration (NASA), and space agencies around the World. As the missions to Mars become more massive and more complex, advanced technologies and new approaches must be utilized to assure the success and contain the costs of the entire Mars program. When the time comes to send humans to the red planet, aeroassist maneuvers will most certainly be required to make such an ambitious mission possible.

1.1 Background of Aeroassist Maneuvers

Aeroassist maneuvers are any in which a spacecraft travels through the atmosphere of a planet for the purpose of using the forces created by the atmosphere acting on the body for some net gain. The chronicle of Mars aeroassist began with the Viking missions of 1976, when each of the two landers left parking orbits and entered the atmosphere. The resulting drag exerted onto the landers helped slow them to a speed for a safe parachute deployment and soft landing (Reference 1). In 1997, the Mars Pathfinder mission employed a similar technique by performing a direct entry into the atmosphere from a hyperbolic arrival trajectory. This eliminated the requirement of a propulsive (using chemical rockets) velocity change (ΔV) to slow the spacecraft enough to be captured into a parking orbit (Reference 2).

Aeroassist maneuvers for orbiting spacecraft at Mars were first demonstrated by Mars Global Surveyor (MGS) in 1997. Upon arrival at Mars, a propulsive ΔV was performed to change the MGS orbit from hyperbolic to elliptic. Once captured into a Mars orbit, the spacecraft passed through the upper atmosphere near the periapsis of each orbit. The drag exerted on the spacecraft removed some orbital energy and reduced the eccentricity of the orbit during each pass. This aerobraking was continued until the desired circular parking orbit was achieved, greatly reducing the amount of fuel that would have otherwise been required for the same orbit (Reference 3).

Aerocapture is a combination of both direct entry and aerobraking that has not yet been demonstrated, but has potential for additional fuel mass savings for future missions. In this maneuver, a spacecraft would enter the atmosphere directly from the hyperbolic arrival



trajectory. Instead of becoming completely captured in the atmosphere and continuing down to the surface as in direct entry, the spacecraft would exit the atmosphere again similar to aerobraking. The goal is to use atmospheric drag to remove enough energy that when the spacecraft exits the atmosphere it will be in the desired elliptic orbit. A small propulsive ΔV would then be performed at apoapsis to raise the periapsis out of the atmosphere or circularize the orbit.

1.2 Spacecraft Guidance Routines

Any unpiloted vehicle at Mars requires an autonomous guidance algorithm to accurately reach a targeted final state at the end of a trajectory. In the case of Mars exploration, this includes precision landing at a predetermined site, or achieving the desired orbit following aerocapture. The guidance algorithm commands changes to the vehicle orientation to assure that the target state is reached. The guidance system collects information about the current state of the vehicle from the navigation system and sends commands to the control system.

For aeroassist maneuvers, guidance algorithms make use of the aerodynamic forces exerted onto the vehicle. In nonballistic trajectories, these forces may be represented by orthogonal vectors lift and drag (assuming the spacecraft produces no net sideforce). By changing the relative orientation of the vehicle, the direction of these force vectors may be adjusted to alter the motion of the spacecraft to modify the trajectory. For aerocapture, drag is essential to removing orbital energy while lift becomes the major control force for targeting the desired exit state.

Many different approaches to the guidance problem have been studied and demonstrated to work for a variety of aeroassist maneuvers. One such method is a numerical predictor-corrector. This algorithm contains the essential models (vehicle, gravity, and atmospheric) on board the spacecraft to numerically integrate the equations of motion in real time and predict the remaining portion of the trajectory. Comparisons are then made with the target state, and control commands are sent to correct any error. This approach has the advantage of being very robust, but can be complicated and computationally expensive (Reference 4).

Another type of guidance algorithm uses a predetermined nominal trajectory as a reference to target a desired final state. Control forces may be used to attempt to return to the target when off nominal conditions cause deviations. An example of this is the guidance algorithm used for Earth reentry of the Apollo missions. Many derivatives of the Apollo algorithm exist, including aerocapture versions. Terminal control theory is used to target the final state upon atmospheric exit. The advantage of the Apollo derived method is its relative simplicity, however the results are heavily dependent on the selection of the reference nominal trajectory (Reference 5).

1.3 Application of Guidance to Aerocapture

A proven robust method for Martian aerocapture guidance is a bank reversal algorithm (Reference 5). This approach controls the spacecraft orientation about a single axis. For this study it is assumed that the aerodynamic moments on the vehicle balance such that the angle of attack (α) and sideslip angle (β) are constant. This leaves bank angle (ϕ) as the control parameter. Because bank angle is measured about the velocity vector, and the lift vector is perpendicular to the velocity vector, changing bank angle results in a change in the lift vector direction. Bank changes may be achieved with onboard reaction jets, reaction wheel, or some other method.

Targeting to a desired final orbit during an aerocapture maneuver means achieving certain predetermined orbital parameters upon atmospheric exit. Given bank control only, it is possible to target apoapsis altitude (h_a) and inclination angle (i) of the resulting orbit. For any bank angle, the lift vector may be divided into a component along the position vector measured from the center of the planet to the vehicle ("vertical") and orthogonal to both the position vector and the velocity vector ("out of plane"). The magnitude of the vertical component affects apoapsis altitude, while the magnitude of the out of plane component affects inclination angle. The apoapsis altitude is a reflection of the orbital energy. For a given initial flight path angle, the vertical component of lift controls how deep the vehicle will go into the atmosphere, in turn affecting how much drag is exerted (and how much energy is removed). The out of plane component of lift changes inclination by rotating the angular momentum vector.

The bank reversal scheme focuses on commanding changes in the bank angle to adjust the vertical component of lift for targeting the apoapsis. The out of plane component of lift then causes the vehicle to drift from the desired inclination angle. When the deviation becomes too great, a bank reversal is performed. By reversing the sign of the bank angle the out of plane component points in the opposite direction, resulting in a reduction of the inclination angle deviation, while the vertical component remains unchanged. By defining an inclination angle corridor, the deviations at which bank reversals are performed gradually reduce over the length of the trajectory such that the final deviation in inclination angle becomes acceptable.

Any control actuation for vehicle orientation will have a limit on the angular acceleration. Many control systems also have a rate limits. Both rate and acceleration limits are included in the bank angle control used in this study. The conclusions remain the same if the rate limit constraint is lifted.

With these constraints, a bank reversal will take some finite time during which the lift vector will not be pointed in the nominal direction. While the vertical component of lift is mainly used to control the final apoapsis altitude, it also has an affect on the periapsis altitude (h_p). Because the final periapsis altitude following aerocapture can never be above the atmosphere, a propulsive ΔV must be performed at the first apoapsis. To minimize the required ΔV for minimum fuel requirements, it is desirable to maximize the final periapsis altitude. While performing a bank reversal there are two options for which direction to bank, through zero degrees ("lift up") or through 180 degrees ("lift down"). The final periapsis altitude may be increased by simple banking different directions during certain portions of the trajectory.

An additional advantage of a higher periapsis relates to mission robustness. For example, if a malfunction caused the circularization burn not to execute following aerocapture, a higher periapsis altitude reduces the orbit decay rate. If the periapsis is high enough, several orbits may be survivable, allowing several more chances at circularization. A safe periapsis altitude is unique to each mission depending on vehicle and mission design as well as robustness criteria. However, it is doubtful that such a high periapsis altitude can be achieved with aeromaneuvering alone.

2 Angular Motion Simulation

Trajectory simulations are performed by numerically integrating the equations of motion with respect to time. A six degree-of-freedom (6-DOF) simulation integrates both the translational and rotational equations, while a three degree-of-freedom (3-DOF) simulation integrates the translational equations only. It is less computationally expensive to perform a 3-DOF simulation than a 6-DOF simulation due to the reduced number of equations to be integrated. Because the assumption is made in this study that the angle of attack and sideslip angle will remain constant, it is not necessary to evaluate the rotational equations in the simulations. A 3-DOF simulation can be used to demonstrate the methods, while a 6-DOF simulation could be used for final verification. The remaining rotational parameter, bank angle, is commanded rather than solved for. Therefore, only a 3-DOF simulation is performed for this study.

The relative vehicle orientation is important in determining the correct aerodynamic coefficients and the direction of the forces action on the vehicle. The bank angle is assumed to be controlled by the reaction control system (RCS) and subject to finite maximum rates and accelerations. Simply commanding a new bank angle in a 3-DOF simulation will result in instantaneous bank angle changes. While this assumption provides advantages for analytical analysis, it is not representative of actual vehicle motions. A bank dynamics model may be included in the simulation to limit the bank rate and acceleration to preset values. This has the effect of including realistic angular motion to a 3-DOF simulation without adding much computational complexity.

2.1 Method Development

The model controls the bank angle provided to the rest of the simulation, but does not simply set the bank angle to the command angle. Instead, the bank acceleration is commanded and a new bank angle and bank rate are calculated from the acceleration. Because the simulation is solved over discrete time steps, the correct acceleration cannot be calculated directly from the continuous time rotational motion equations. It is assumed that the bank acceleration is constant throughout one time step and may be instantaneously changed from one time step to the next.

When a bank change command is given, rotation toward the command angle is started by setting the acceleration to the maximum allowable value in the proper direction. This acceleration is held constant until the maximum allowable bank rate is reached or the command angle changes. Setting the acceleration to zero at any time will result in the bank angle continuing to change at a constant rate.

The discrete time steps cause difficulties in properly commanding a deceleration to stop at the commanded bank angle without overshooting. To set the correct deceleration command, the bank angle through which the vehicle would travel before reaching zero bank rate (stopping), given the maximum deceleration, is constantly monitored. The stopping angle is then calculated as the current bank angle plus the stopping distance. Because of the discrete time steps, this is always done one time step in advance to prevent an overshoot of the commanded bank angle. For example, if the maximum acceleration is commanded, to be held constant, the final bank angle may stop short of the command bank angle. But if the maximum acceleration is commanded one time step later, it may overshoot. Therefore, the stopping angle is predicted in each time step if the maximum acceleration were commanded starting one time step later.

An illustration how the discrete time motion compares to continuous time motion is shown in Figure 2.1.

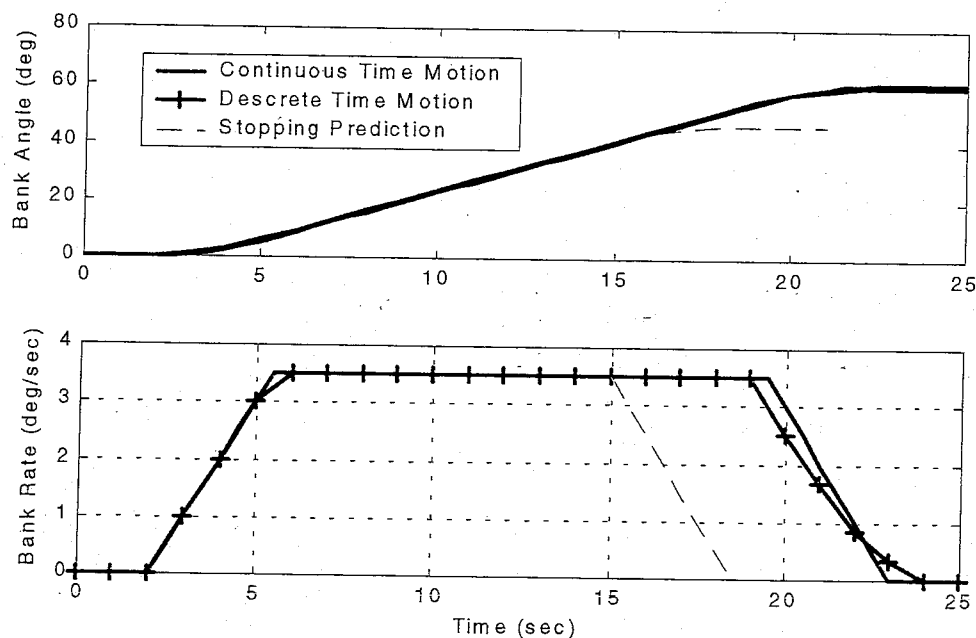


Figure 2.1: Bank Dynamics Model Compared to Continuous Time Motion

Figure 2.1 illustrates the motion for a 60 degree bank change command (issued at time=2 sec) with a maximum bank rate of 3.5 deg/sec and a maximum bank acceleration of 1 deg/sec². Each time interval is 1 sec in length. Because the continuous time accelerations change in between time steps, the dynamics model must calculate accelerations one interval in advance. It can be seen how the deceleration to the command angle begins early to prevent an overshoot, and the deceleration rate is adjusted to meet the command angle. The dotted lines represent how the stopping angle is continuously monitored throughout the motion.

The predicted stopping distance is found from the following constant acceleration rotational motion equations:

$$\phi(t + \Delta t) - \phi(t) = \dot{\phi}(t)\Delta t + \frac{1}{2}\ddot{\phi}(t)\Delta t^2 \quad (2.1)$$

$$\dot{\phi}(t + \Delta t) - \dot{\phi}(t) = \ddot{\phi}(t)\Delta t \quad (2.2)$$

Because stopping is defined by bank rate reducing to zero, the change in bank rate is simple the opposite of the current bank rate ($\Delta\dot{\phi} = -\dot{\phi}$). By solving Equation 2.2 for Δt and substituting the result into Equation 2.1, the stopping distance is found to be:

$$\Delta\phi = \text{sign}[\dot{\phi}(t)] \frac{\dot{\phi}^2(t)}{2\ddot{\phi}_{\max}} \quad (2.3)$$

To project one time step ahead, assuming no change in the acceleration, Equations 2.1 and 2.2 are used where the time interval is equal to the duration of a single time step ($\Delta t = dt$). The stopping angle, given a maximum deceleration beginning one time step later, is then predicted by:

$$\phi_{\text{stop}} = \phi(t) + \dot{\phi}(t)dt + \frac{1}{2}\ddot{\phi}(t)dt^2 + \text{sign}[\dot{\phi}(t) + \ddot{\phi}(t)dt] \frac{[\dot{\phi}(t) + \ddot{\phi}(t)dt]^2}{2\ddot{\phi}_{\max}} \quad (2.4)$$

If this predicted stopping angle overshoots the command angle, then the maximum bank deceleration is commanded. Because the prediction was made one time step in advance, commanding the maximum deceleration in the current time step (to be held constant until the rate reaches zero) will insure an undershoot. If the bank command changes then the acceleration is calculate based on the new command angle,

A tolerance margin is assumed near the commanded bank angle within which the prediction is not needed. This margin is the distance that could be traveled in a single time

step, starting from rest, for a maximum acceleration. It is calculated by Equation 2.1 assuming the bank rate is zero ($\dot{\phi} = 0$) and the time interval is equal to the duration of one time step ($\Delta t = dt$).

Once the deceleration has begun, the stopping angle is still constantly monitored to calculate adjustments to the deceleration rate for convergence to the command angle. The maximum deceleration is commanded whenever the predicted stopping angle overshoots the commanded angle. If the stopping angle is predicted to undershoot the command angle, then the deceleration command is reduced such that a zero bank rate should be achieved at the commanded bank angle. The non-maximum deceleration rate is found by solving Equation 2.2 for Δt , substituting it into Equation 2.1 and solving for the deceleration. The resulting equation is as follows:

$$\ddot{\phi}_{cm} = \frac{-\dot{\phi}^2(t)}{2[\phi_{cm} - \phi(t)]} \quad (2.5)$$

For all other cases, the bank acceleration is calculated as follows:

$$\ddot{\phi}_{cm} = \frac{\dot{\phi}_{cm} - \dot{\phi}(t)}{dt} \quad (2.6)$$

2.2 Flow of Bank Dynamics Model

It is assumed that the bank angle will be considered between -180 and $+180$ degrees only. All angles calculated outside these limits are adjusted by multiples (if necessary) of 360 degrees such that they will remain within the bounds.

A flow chart of the model is provided in Appendix A. The bank dynamics model first calculates the predicted stopping angle and the tolerance margin by Equation 2.4 and Equation 2.1 respectively. Next, the required bank angle change is calculated. The general method is to calculate the difference between the current bank angle and the commanded bank angle as follows:

$$\delta\phi = \phi_{cm} - \phi(t) \quad (2.7)$$

Equation 2.7 is modified to account for the desired bank direction. This is done by adding or subtracting 360 degrees depending on the sign of the bank angle change and desired direction. In the case where the bank angle is close to the command bank angle

(within 5 degrees for example) the commanded direction is ignored and Equation 2.7 is used in its unchanged form for preventing overshoots caused by command angle changes.

Next, the desired bank rate is calculated by dividing Equation 2.7 by one time interval (dt). The equation is as follows:

$$\dot{\phi}_{cm} = \frac{\delta\phi}{dt} \quad (2.8)$$

This is the equivalent of attempting to reach the commanded bank angle in a single time step. The commanded rate is then limited such that it does not exceed the maximum allowable rate.

Next, the predicted stopping angle is monitored for an overshoot. To check for a predicted overshoot is complicated due to the ± 180 degree discontinuity. If it indicates an overshoot, and the command angle has not changed, the deceleration rate is calculated.

The commanded acceleration rate is calculated by Equation 2.6 unless the deceleration has begun. Notice that this, similar to the rate equation, is equivalent to attempting to reach the commanded rate in a single time step. It too is limited such that it will not exceed the maximum allowable value set by the user. If the deceleration has started and the predicted stopping angle overshoots the command angle, then an acceleration rate is commanded to begin stopping the motion using Equation 2.6 where the command rate is zero ($\dot{\phi}_{cm} = 0$). Otherwise, if the deceleration has started and the predicted stopping angle undershoots the command angle, then a smaller acceleration rate is commanded using Equation 2.5. Similar to the adjustment made to the rate command, this equation is modified to account for the ± 180 degree discontinuity and is as follows:

$$\ddot{\phi}_{cm} = \frac{-\dot{\phi}^2(t)}{2\delta\phi} \quad (2.9)$$

where the angle difference of the denominator is given by Equation 2.7 and has already been modified.

Once the acceleration command is calculated and limited, the new bank angle is calculated by Equation 2.1. Finally the new bank rate is calculated by Equation 2.2. In both cases, the time interval is equal to the duration of one time step ($\Delta t = dt$).

2.3 Application to Simulation

When the bank dynamics model is included in the aerocapture simulation, the effects are most noticeable when bank reversals are performed. When the guidance algorithm is commanding slight adjustments to the bank angle to account for deviations from the nominal trajectory, the motions are small enough that the rates rarely reach the allowable limits. For bank reversals, however, large angular distances are traversed and it becomes apparent that the motion resembles the results of solving the rotational equations.

Before including the bank dynamics model into the simulation it was tested to identify and resolve any unexpected behavior. A series of bank angle commands were tested for various bank direction commands, and the angle was monitored for overshoots and how closely it followed the commands. This was performed for assorted rate and acceleration limits. A sample test case is shown in Figure 2.2.

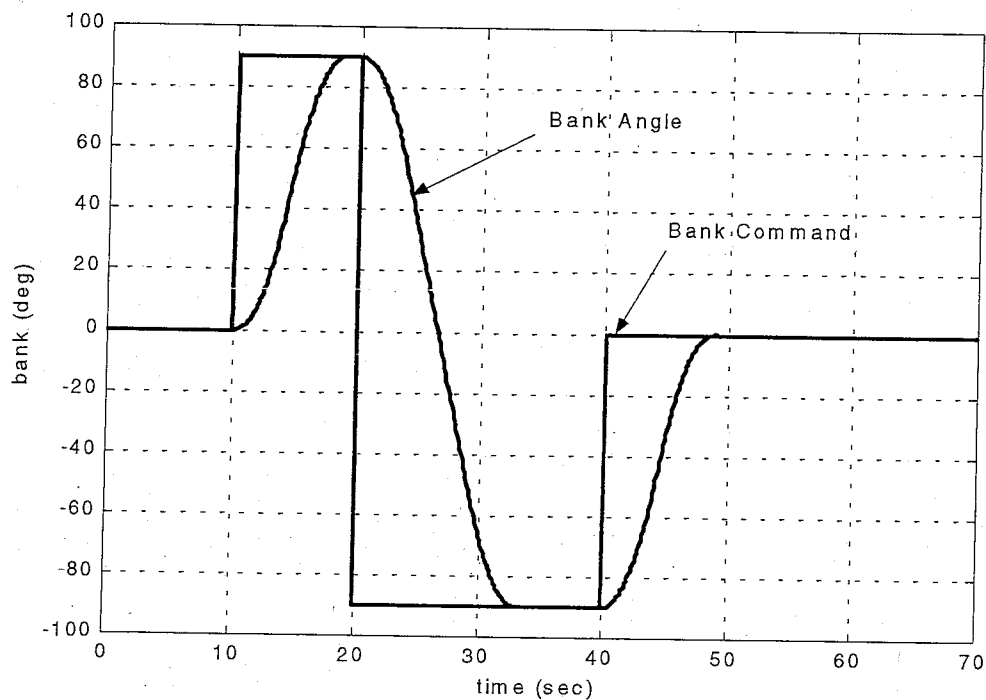


Figure 2.2: Sample Bank Dynamic Model Test Case

3 Simulation Development

To develop, analyze, and evaluate the guidance algorithm bank reversal control logic, an existing, universal, computer based simulation was utilized. The Program to Optimize Simulated Trajectories (POST) is used to solve the general equations of motion to generate vehicle trajectories near an arbitrary, oblate planet. Propulsive, aerodynamic, and gravitational forces acting on the vehicle are included depending on the specific simulation. The vehicle is considered as a point mass for 3-DOF simulations. A targeting and optimization routine may be employed to determine the value of any number of independent parameters needed to meet certain constraints (Reference 6).

3.1 POST General Simulation Solutions

It is possible to solve a wide range of very complicated problems using POST due to flexibility in input structure. Problem specific information may be input in a variety of different reference frames and the program will internally convert everything into a common reference frame. For example, vehicle characteristics like orientation, aerodynamic coefficients, and propulsive forces may be input in a body fixed coordinate frame. All reference frame dependent data is converted to a planet centered inertial frame in which the equations of motion are integrated.

The translational equations of motion in the inertial coordinate system are directly derived from Newton's second law of motion. These equations, from Reference 6, are as follows:

$$\dot{\vec{r}} = \vec{V} \quad (3.1)$$

$$\dot{\vec{V}} = [IB]^{-1}(\vec{a}_T + \vec{a}_A) + \vec{g} \quad (3.2)$$

where the thrust acceleration and the aerodynamic acceleration are represented in the body frame, and IB is a transformation matrix from the inertial frame to the body frame.

The equations of motion represent the basic dynamics universal to every POST simulation. Problem specific information alters these equations by different position and velocity initial conditions and through different acceleration values. The POST input structure provides a means for this information to be collected by the dynamics solver. The flow of the complete POST simulation solution is represented in Figure 3.1 (Reference 7).

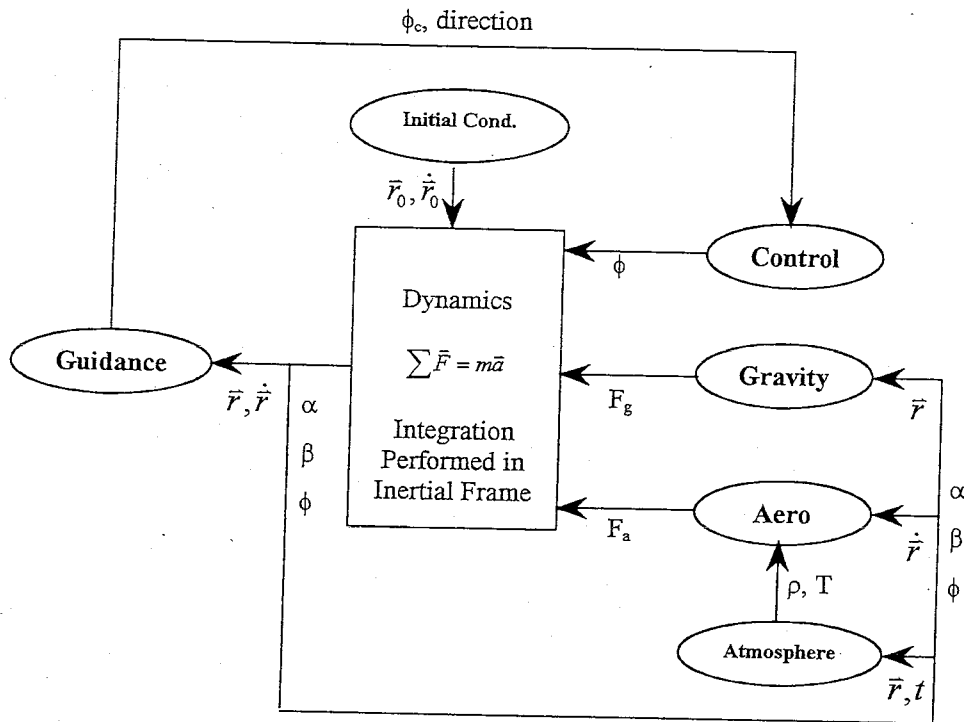


Figure 3.1: Flow Diagram of POST 3-DOF Simulation (Reference 7)

The bank angle control variable is provided to the simulation, but is not directly included in the integration. It is included indirectly, however, by influencing the direction of the aerodynamic forces. All of the supporting models define a unique simulation.

3.2 Mars Aerocapture Specific Simulation Input

For this study, the current reference human mission architecture is used to develop the simulation. The simulation then is built upon realistic data of a potential vehicle and mission. Architecture information and vehicle data are obtained from Reference 8 and Reference 9, including arrival conditions such as position and velocity relative to a Mars centered inertial coordinate system. Detailed aerodynamic coefficients (Reference 10) dependent upon Mach number (M), angle of attack (α), and sideslip angle (β) are used for aerodynamic force calculations.

The Mars version of 3-DOF POST contains specific Mars gravity and atmospheric information and is used for the simulation solutions. The production version contains options for existing atmospheric and gravitational models. The Mars gravity model used for this

study consists of the gravitational parameter (μ) and the second zonal harmonic coefficient (J_2) to account for planet oblateness. Equatorial and polar radii are input as well for calculating geodetic parameters. Also, the rotation rate (Ω) of the planet is included for transformations to a surface fixed reference frame needed for calculations dependent on vehicle longitude and latitude. These data are obtained from Reference 11.

The atmospheric model used is the Mars Global Reference Atmospheric Model (Mars-GRAM). Mars-GRAM is a commonly used model for Mars trajectory simulations using POST. It is derived from data collected by the Mariner and Viking missions. Local and seasonal variations are accounted for; therefore the data is dependent on longitude, latitude, and time (Reference 12). An arrival date of the first of July, 2014, corresponding to the first opportunity for the reference human mission (Reference 8), is used. A representation of the vehicle aerodynamic characteristics is shown in Figure 5.2. The significant information needed to create this specific simulation is provided in Table 3.1.

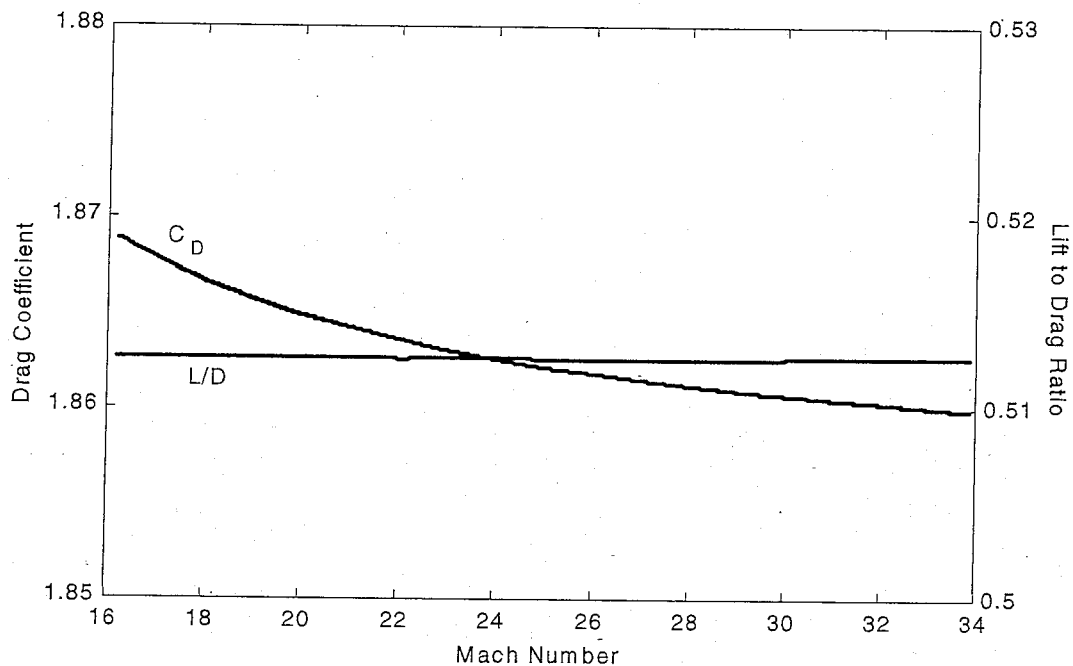


Figure 3.2: Illustration of Vehicle Aerodynamic Characteristics

Table 3.1: Reference Mars Mission Specific Simulation Data

Equatorial Radius	r_e	3,393.94	km
Polar Radius	r_{polar}	3,376.78	km
Gravitational Parameter	μ	4.28282868534e13	m^3/sec^2
Rotation Rate	Ω	7.088218e-5	rad/sec
Second Zonal Harmonic	J_2	1.9595e-3	~
Arrival Julian Date	JD	2456839.5	yr
Vehicle Mass	m	85,000	kg
Reference Area	S_{ref}	84.3	m^2
Reference Length	l_{ref}	23.0	m
Lift to Drag Ratio	L/D	0.5126	~
Angle of Attack	α	45.0	deg
Sideslip Angle	β	0.0	deg
Entry Velocity	V	5900	m/s
Entry Longitude	Long	0.0	deg
Entry Latitude	Lat	-15.15	deg
Entry Altitude	h	129,000	m
Maximum Mach Number	M	34	~
Minimum Mach Number	M	16	~

The preliminary nature of a human mission to Mars, and the associated data, is not a factor in the overall results of this study. The results examined here seek to define and document general trends that may be encountered in any Mars aerocapture maneuver. Discovery of these trends fits with the advanced concepts sure to be exploited in a human mission. The use of this data adds to the legitimacy of the simulation. To verify that no significant errors have been made in the generation of the essential elements of the basic simulation, the results have been compared with those provided in Reference 9. Because minimum data is included in Reference 9, general comparisons were made between the trajectories and similar trends were observed.

4 Bank Reversal Control Logic

Bank reversal control logic is commonly applied to aeroassist problems because it provides control for two dependent parameters (inclination and apoapsis altitude) through one independent parameter, bank angle. This requires the spacecraft control system to monitor and control the vehicle orientation about a single axis only, while the orientation about the remaining two axes stays constant. Control of an aerodynamic angle, such as bank angle, considers the relative orientation of the body-fixed stability axes. Lift produced by the vehicle can be used as the control force for precision targeting. The proposed ellipsed configuration for the reference human mission is a relatively high lift to drag ratio (L/D) configuration compared to previous atmospheric entry vehicles (Reference 9). This provides adequate control authority for precision targeting.

The aerodynamic forces acting on the vehicle considered in this study are depicted in Figure 4.1. Note that the illustrated flight path angle (γ) represents a negative value. The vehicle configuration and mass distribution is designed such that the aerodynamic moments balance to a constant angle of attack providing the desired L/D . The drag force removes kinetic energy by acting opposite the relative velocity vector. The magnitude of the drag force is strongly dependent on the density (ρ) of the atmosphere, which is primarily a function of altitude. The vertical component of the lift vector is used to control the magnitude of the drag force by controlling how deep into the atmosphere the vehicle will fly.

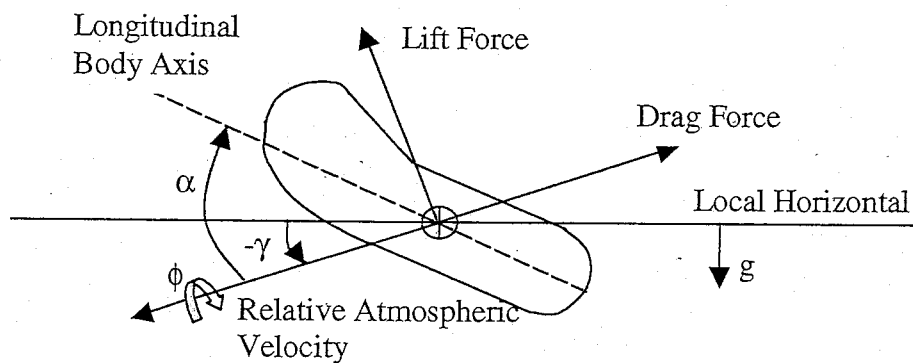


Figure 4.1: Aerodynamic Forces Acting on High L/D Vehicle

Bank angle is measured about the x-axis of the stability coordinate system. In this system, the x-axis coincides with the velocity vector; therefore a change in bank angle has no direct influence on the direction of the velocity or drag vectors. A transformation matrix from the body fixed stability axes to a local vertical local horizontal (LVLH) system is used to find the components of the lift force. Both the flight path angle (γ) and bank angle (ϕ) must be considered.

The out of plane force component is the portion of the lift force not contained in the orbital plane and as a result causes the inclination angle to change. The magnitude of the out of plane force component is not directly available to the control system as an independent parameter because the bank angle is controlled to adjust the vertical component for apoapsis targeting. However the sign of the bank angle may be independently controlled to change the direction of the out of plane force component for inclination targeting.

4.1 Aerocapture Simulation Boundary Condition Definition

The initial state of the vehicle strongly influences the bank angle profile needed to reach the desired final state. The initial flight path angle (γ) defines the vertical component of the initial velocity vector and affects the altitude of closest approach. For a given longitude and latitude the initial azimuth angle (a_z) defines the initial inclination of the orbit. If no out of plane force is applied to the vehicle, the inclination will remain nearly constant throughout the trajectory except for small drifts toward smaller inclination angles due to rotation of the planet atmosphere (Reference 5).

These two independent initial parameters are studied to define a range of values in which the desired trajectory may be flown. The smallest and largest initial flight path angles possible, with the control authority to still target the desired apoapsis altitude, define the entry corridor. If zero bank angle is held constant throughout the trajectory (full lift up), the initial flight path angle must be steep to target apoapsis. Conversely, if a bank angle of 180 degrees (full lift down) is held constant, the initial flight path angle must be shallower to target the same apoapsis altitude. Likewise, an initial azimuth angle must be chosen to account for the inclination drift produced by out of plane forces.

A diagram of a general approach and aerocapture trajectory is shown in Figure 4.2.

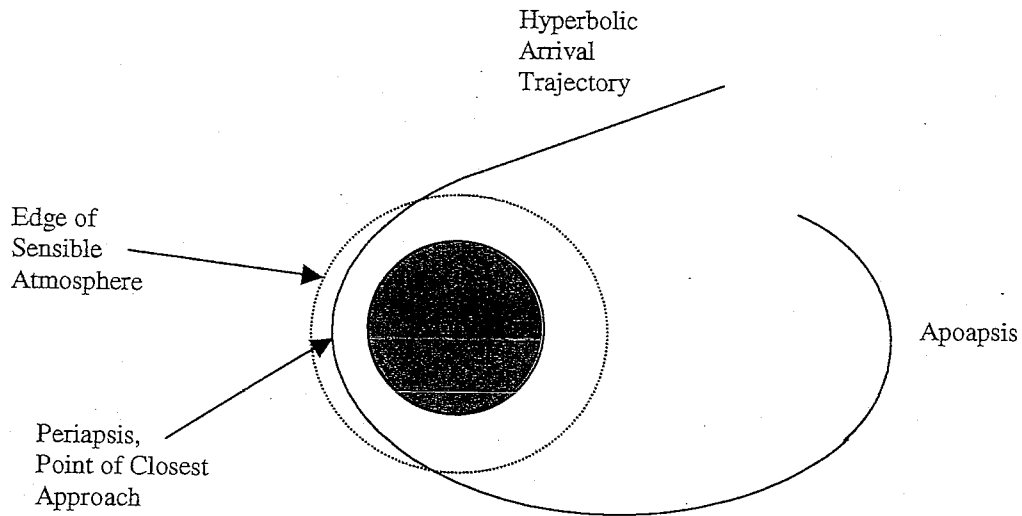


Figure 4.2: Diagram of General Aerocapture Trajectory

Initial conditions are defined at the edge of the sensible atmosphere ($h = 190$ km). The simulation calculates the trajectory between atmospheric entry and exit. The orbital elements at atmospheric exit may be used to propagate the final orbit. A target exit apoapsis altitude of 600 km and inclination angle of 45 degrees is chosen for this study.

To define the entry corridor, a constant lift up or lift down orientation is specified, and the initial flight path and azimuth angles are varied until the final apoapsis and inclination targets are reached. To expedite this process, the targeting/optimization feature of POST was used. The projected gradient method included in POST will vary a set of independent control parameters from an initial guess until a set of dependent constraints are met. A complete description of this process is available in Reference 6. This feature has been used extensively throughout this study for iterating on independent input parameters to find trajectories with the desired results.

In this case, the control parameters are initial inclination and azimuth angles, while the constraints are that the final apoapsis altitude and inclination angle must be within a specified tolerance of the target values. Because apoapsis altitude is not defined for the non-elliptic portions of the trajectory, it may not be used directly as a constraint. Instead, the constraint is defined as either orbital energy or apoapsis altitude depending on the orbit type. This defines the apoapsis altitude as an equality constraint during the elliptic portion of the

trajectory, and the energy as an inequality constraint everywhere else in the trajectory to drive the energy toward that of an elliptic orbit. Once the boundary conditions of the initial values are defined, average values may be used to develop the reference nominal trajectories.

4.2 Definition of Bank Reversal Boundaries

For trajectories in which a out of plane force is produced, the direction of the force must be changed to offset the induced inclination drift. As a reference, a ballistic entry trajectory (zero lift) was simulated. The initial azimuth angle was chosen to meet the target inclination, and the history of the inclination angle throughout the trajectory was recorded. As expected, a drift of about one degree toward lower inclination was present. This reference was used to monitor inclination drift from nominal caused by the out of plane force component of lift.

A nominal bank angle of 90 degrees was chosen for this study. It was found that the final periapsis altitude is very sensitive to the magnitude and direction of the vertical component of lift. By choosing a nominal orientation with no vertical component, it is assured that the bank reversals performed in the trade studies have the only affect on final periapsis altitude and not the selection of a nominal angle. Because this orientation produces so much lift in the out of plane direction, the vehicle will diverge from the reference inclination rapidly. When the deviation between the inclination angle and the reference inclination angle becomes too large, a bank reversal is performed. By reversing the direction of the out of plane force, the inclination will then converge back toward the reference angle.

The direction the inclination angle changes due to the direction of the out of plane force is dependent on whether the vehicle is ascending or descending in the orbit. The initial state used in this study describes the ascending portion of the orbit. For all simulations, a positive bank angle producing an out of plane force will result in decreasing the inclination angle, while a negative bank angle will cause the inclination angle to increase.

The initial bank angle in all simulations performed in this study is positive. Three reversal scenarios where examined to determine which yielded the highest final periapsis altitude. Inclination boundaries were defined to simulate trajectories containing one, two, and three bank reversals.

4.2.1 One Bank Reversal

The simplest trajectory examined requires only a single bank reversal. The reference inclination history is included in the simulation to be used in calculations. The POST targeting feature is provided with the final apoapsis altitude and inclination as constraints. The initial azimuth angle is the same as that in the reference ballistic trajectory, and the control parameters are the initial flight path angle and the time of the bank angle reversal.

The bank angle is held constant at 90 degrees until the deviation between the inclination angle and the reference inclination (Δi) reaches some value, and then the bank angle is switched to -90 degrees. The magnitude of the maximum allowable deviation is chosen by the targeting routine to meet the final inclination constraint. A history of key parameters for this trajectory is shown in Figure 4.3.

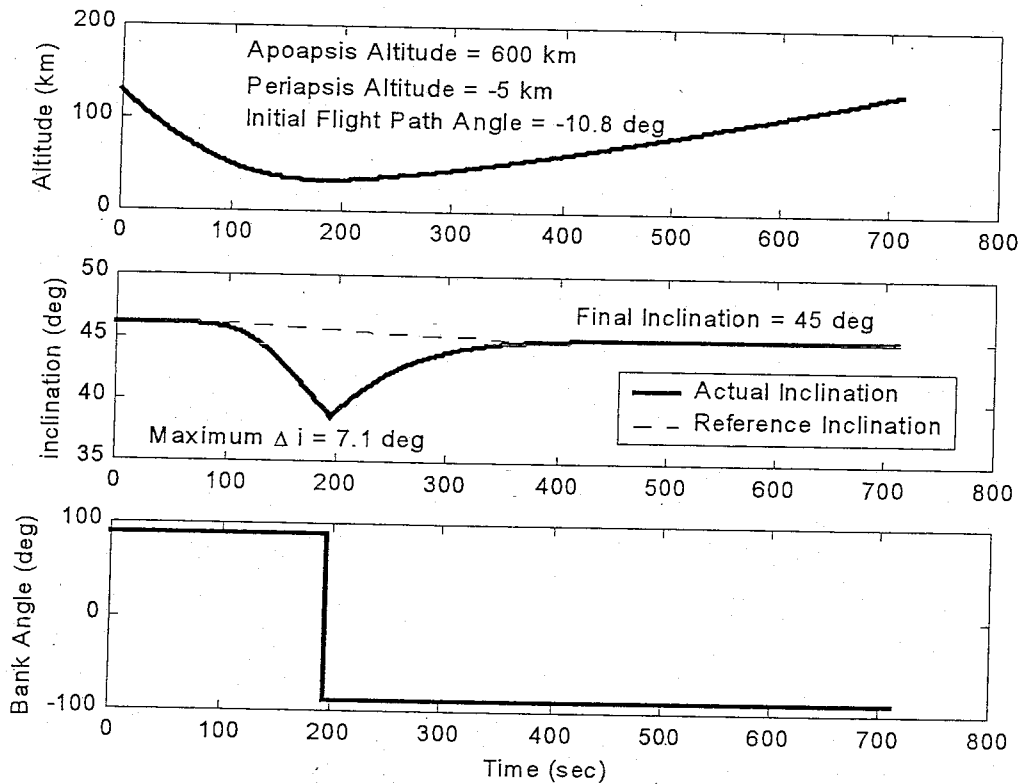


Figure 4.3: Single Bank Reversal Reference Trajectory

Notice that the bank angle instantaneously switches sign. Throughout this study, simulations allowing instantaneous bank angle changes have been continuously referred to as

a reference for those using the realistic bank dynamics. Figure 4.3 represents one of the many reference trajectories.

4.2.2 Two Bank Reversals

The simulation of a trajectory containing two bank reversals is similar to that for a single reversal. The targeting routine is used to iterate the magnitude of the inclination deviation at the first reversal to reach the final inclination. The magnitude of the inclination deviation at the second reversal is defined as a ratio of the inclination deviation at the first reversal.

For example, the inclination will deviate from the nominal until the magnitude of the deviation reaches the value calculated by the targeting routine. A reversal will be performed, and the inclination angle will return toward the nominal angle. The deviation will decrease until the inclination crosses the nominal. The magnitude of the deviation is allowed to increase from there until it reaches a value equal to a multiple of the first maximum deviation value. Following the second reversal, the inclination deviation will decrease to zero at the termination of the trajectory. The deviation ratio is defined by the user for trade studies and iterations.

Because the nominal bank angle is 90 degrees, and the reversals are performed instantaneously, the selection of the deviation ratio has little effect on the final state in terms of periapsis altitude. The effects of bank reversals on periapsis altitude become more noticeable as the simulation becomes more realistic.

A history of key parameters for this trajectory is shown in Figure 4.4.

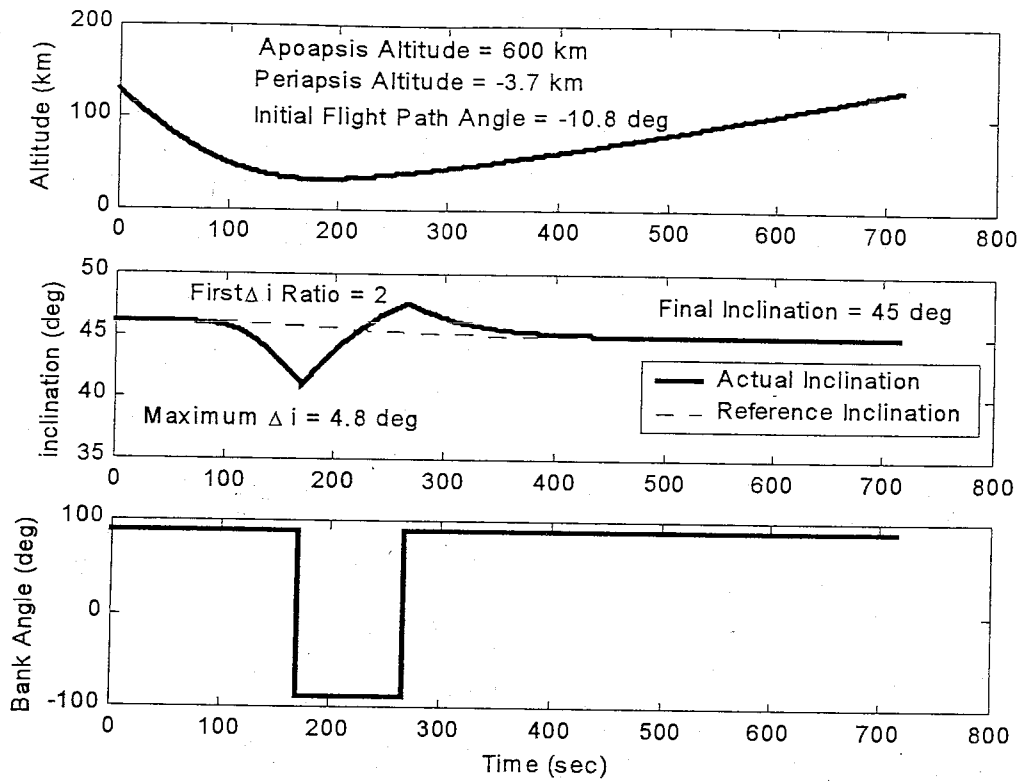


Figure 4.4: Double Bank Reversal Reference Trajectory

4.2.3 Three Bank Reversals

The simulation of the three-bank-reversal trajectory is an extension of the previous one for two reversals. For this case, a second inclination deviation ratio is defined as that of the second inclination deviation limit to that of the third. A history of key parameters for this trajectory is shown in Figure 4.5.

Comparisons between Figures 4.3, 4.4, and 4.5 show very little difference in the final periapsis altitude. This is to be expected since no vertical component of lift is present in any of the trajectories. Therefore the periapsis altitude cannot be controlled. It is expected that the final periapsis altitude be nearly the same as the altitude of closest approach. For a flyby of a planet where no atmosphere is encountered, this would be true. However, atmospheric drag has the effect of reducing the periapsis altitude as well as the apoapsis altitude. The goal of using a reversal direction control logic is to counter that trend or even reverse it.

By studying bank reversals in terms of deviation magnitudes and ratios, complete control is assured over exactly when those reversals take place. This is ideal for defining nominal trajectories, but becomes too complicated for realistic off nominal applications. With the ideal reversal scenarios defined, polynomials may be fit through the points where reversals occur. The lines will then define a set of boundaries converging toward the target inclination angle. These boundaries are included in the guidance algorithm. Whenever the inclination exceeds one of the limits, a reversal is commanded.

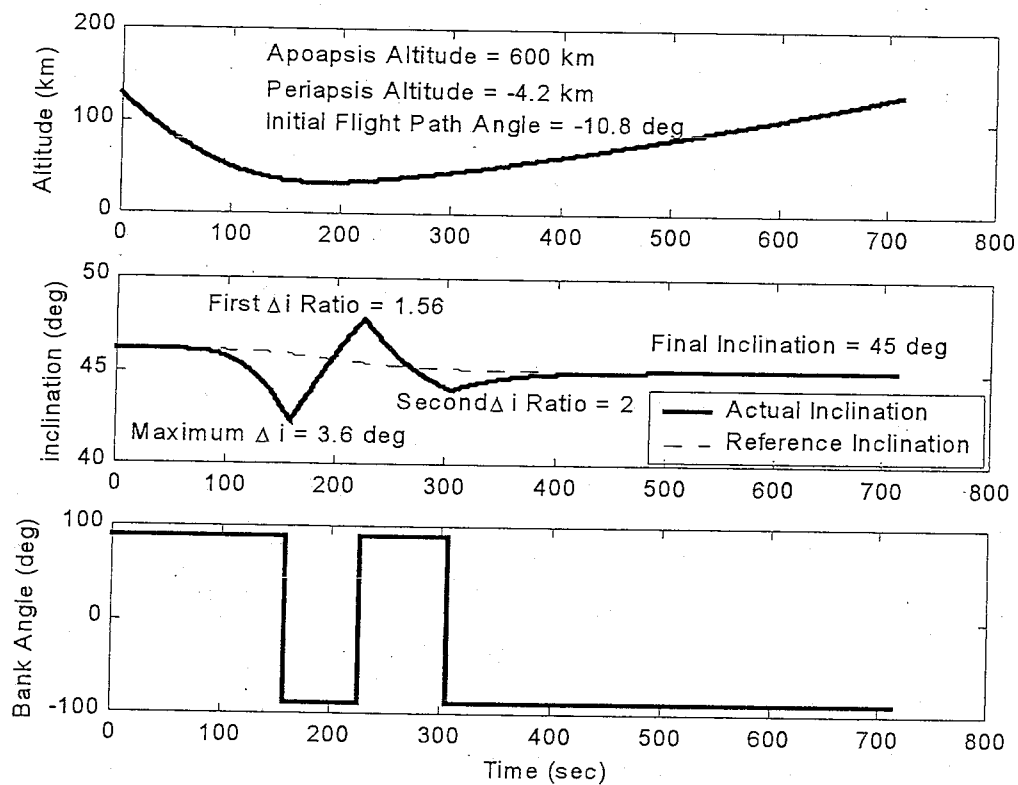


Figure 4.5: Triple Bank Reversal Reference Trajectory

Each of the three reversal scenarios was repeated with realistic bank dynamics once a reversal direction logic was defined. This allowed for the selection of a scenario and inclination deviation ratios to maximize the periapsis altitude. A discussion of this is provided in Section 5.3.1.

5 Bank Direction Control Logic

Employing the bank reversal control method to an aerocapture problem presents another option for a control strategy that may be exploited with minimal added complexity to the controller. Because a nominal bank angle of 90 degrees is assumed, a bank reversal always requires a roll through 180 degrees of rotation. Bank direction is examined here because it has significant affect on the final state of the vehicle, but requires the same level of complexity and RCS propellant.

A general observation that flying full lift down at the end of the trajectory can increase the periapsis altitude has been documented. This is achieved by reducing the flight path angle at atmospheric exit (Reference 5). The same trend was observed in the simulations conducted for this study. The objective then becomes to identify the affects of lift up and lift down forces, applied at different points in the trajectory, on the final periapsis location given the same apoapsis target. -

5.1 Bank Direction Trade Study

The initial approach to identifying a trend was to simulate a trajectory with a single bank reversal similar to that discussed in Section 4.2.1. However, this time the angular motion model was included to simulate realistic bank dynamics. The POST targeting routine was configured to target the final inclination angle and apoapsis altitude while controlling the initial flight path and azimuth angles. This provided appropriate targeting while leaving the bank direction and reversal location available for user specification.

A series of trajectories were simulated for bank reversals at various points in the trajectory. At each reversal location, the bank switch was executed by rolling the lift vector both lift up (through 0 degrees) and lift down (through 180 degrees). In every case, the final state reaches the same apoapsis and inclination. An example of one trajectory with a lift up roll is shown in Figure 5.1. Figure 5.2 shows the corresponding trajectory with a lift down roll.

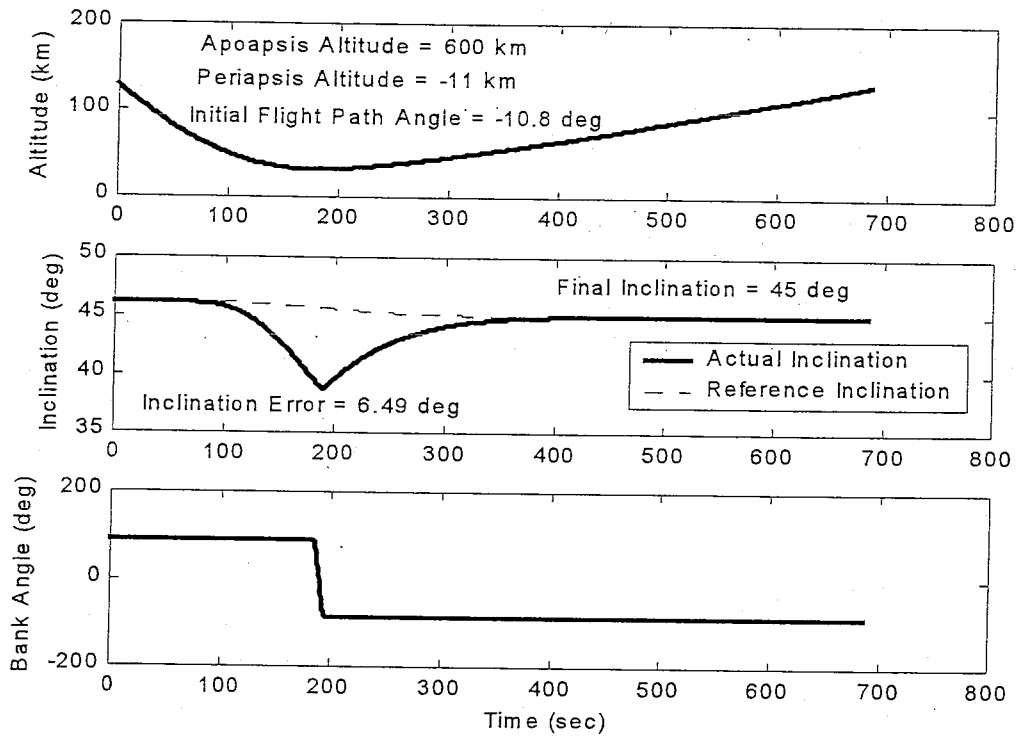


Figure 5.1: Sample Bank Direction Trade Study Trajectory (Bank Through 0 deg)

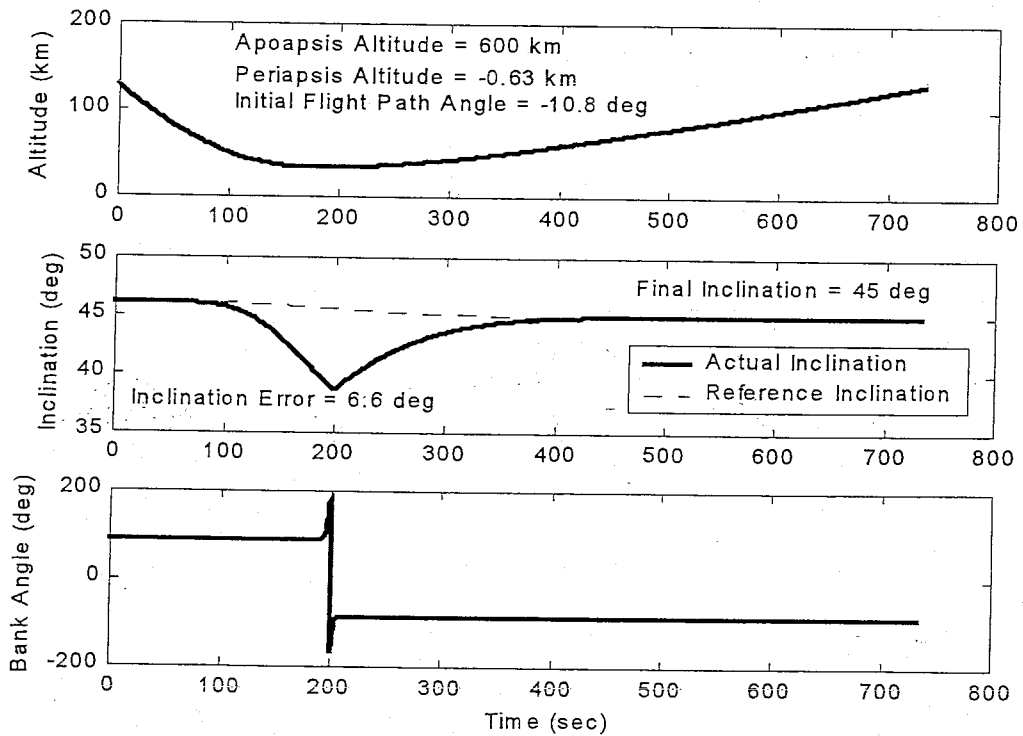


Figure 5.2: Sample Bank Direction Trade Study Trajectory (Bank Through 180 deg)

Notice the apparent discontinuity in the bank angle representation of Figure 5.2. This is due to the numerical representation of the ± 180 degree bounded bank angle assumed for all algorithms included in this study. Also notice the difference in the periapsis of the two trajectories resulting from the different control methods is represented. Figure 5.2 shows an increase of nearly 11 km over Figure 5.1 and approximately 4 km over the instantaneous reversal cases presented in Section 4.2.

The data for each of these trajectories was collected and tabulated to establish trends. Specifically, the final periapsis altitude was examined as a function of the reversal time and direction. A graphical representation of this is provided in Figure 5.3.

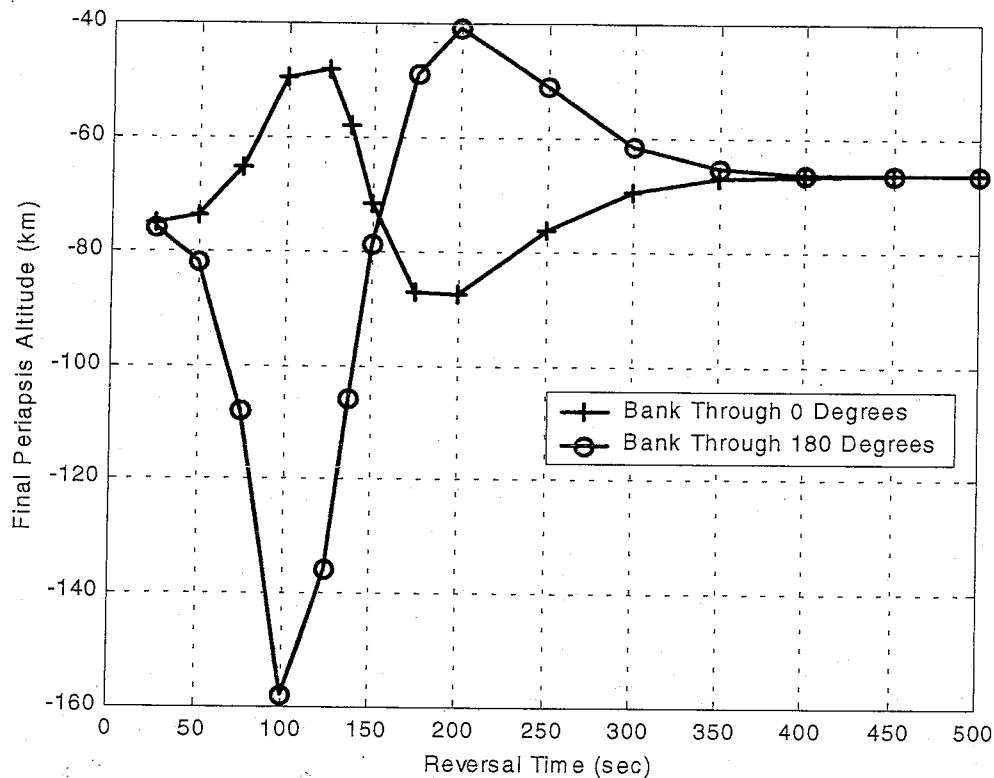


Figure 5.3: Bank Reversal Direction and Location Affects on Periapsis Altitude

The plot indicates that a roll performed lift up in the beginning portions of the trajectory increases the final periapsis altitude, while the final periapsis decreases if it is performed toward the end of the trajectory. Additionally, the opposite is true for rolls performed through lift down. This indicates that performing bank reversals by rolling lift up at the beginning and lift down at the end of the trajectory should increase the final periapsis

altitude. Notice that the trajectories represented in Figures 5.1 and 5.2 contain reversals that occur in what could be defined as toward the end of the trajectory according to Figure 5.1. Indeed, the periapsis altitude is higher for the case rolling lift down.

While this trend agrees with previous thought (that lift down forces near atmospheric exit increase the apoapsis altitude), it does not fully define a relationship between periapsis altitude and the vertical component of lift. Significantly missing from this trade study is the definition of when exactly the benefits switch from lift up forces to lift down forces. Also the differing initial flight path angles between corresponding trajectories means a direct comparison may not be entirely applicable.

5.2 Bank Direction Logic Development

To fully understand and define a relationship, a mathematical representation of the sensitivity of the periapsis altitude to vertical forces was sought. It is assumed that the duration in which the vertical components of lift are present during a bank reversal is short in comparison to the total period of an orbit. This allows the effect of these vertical forces to be compared to impulse accelerations applied to the simulation for verification of the resulting relationship.

5.2.1 Theory Development

To develop a relationship between the periapsis and forces along the direction of lift, the orbital equations for conic sections were considered (Reference 13). The body fixed coordinate system used considers axes along the velocity vector and along the lift vector (orthogonal to velocity). A representation is provided in Figure 5.4.

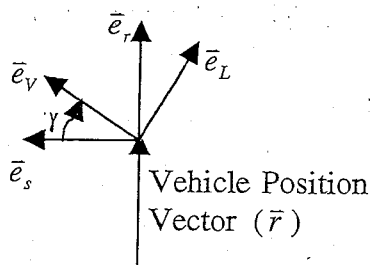


Figure 5.4: Illustration of Body Fixed Coordinate Systems

Unit vectors are represented by \bar{e} with subscripts denoting direction. The development begins with the equation for periapsis radius:

$$r_p = a(1 - e) \quad (5.1)$$

The standard convention is considered where the semi-major axis (a) is positive for elliptic orbits and negative for hyperbolic orbits. Taking the differential of Equation 5.1 yields:

$$\delta r_p = \delta a(1 - e) - a \delta e \quad (5.2)$$

Because forces applied, as a unit impulse in the lift direction (\bar{e}_L), perpendicular to velocity do not change the energy, the differential of the semi-major axis is zero ($\delta a = 0$), and Equation 5.2 simplifies to:

$$\delta r_p = -a \delta e \quad (5.3)$$

Next, the specific angular momentum equation is considered:

$$h^2 = \mu a(1 - e^2) \quad (5.4)$$

Similarly taking the differential of this equation due to a unit impulse in the lift direction results in:

$$2h\delta h = \mu\delta a(1 - e^2) - 2\mu a e \delta e \quad (5.5)$$

Again, using $\delta a = 0$, Equation 5.5 is simplified to:

$$\delta h = -\frac{\mu a e}{h} \delta e \quad (5.6)$$

To form a relationship between the periapsis radius and the specific angular momentum, Equation 5.6 is combined with Equation 5.3 to eliminate the differential of eccentricity (δe). The result is as follows:

$$\delta r_p = \frac{h}{\mu e} \delta h \quad (5.7)$$

Next, the specific angular momentum vector as the cross product of the position and velocity vectors is considered:

$$\bar{h} = \bar{r} \times \bar{V} \quad (5.8)$$

Considering the same impulse perpendicular to the velocity vector and in the orbit plane results in the differential of Equation 5.8 as follows:

$$\delta \bar{h} = \delta \bar{r} \times \bar{V} + \bar{r} \times \delta \bar{V} \quad (5.9)$$

Because an impulse does not change position, the differential of the position vector is zero ($\delta\vec{r} = 0$) and Equation 5.9 simplifies to:

$$\delta\vec{h} = \vec{r} \times \delta\vec{V} \quad (5.10)$$

where the differential of the velocity vector is due to an impulse in the lift direction.

It is convenient to represent the differential of the velocity vector in component form relative to the coordinate frames depicted in Figure 5.4. The result is as follows:

$$\delta\vec{V} = \delta V \cos \gamma \vec{e}_r - \delta V \sin \gamma \vec{e}_s \quad (5.11)$$

Substituting this result into Equation 5.10 results in:

$$\delta\vec{h} = -r \delta V \sin \gamma \vec{e}_s \quad (5.12)$$

Substituting the magnitude of the resulting vector into Equation 5.7 results in the relationship between the periapsis radius and a unit impulse in the lift direction. The equation is as follows:

$$\delta r_p = -\frac{rh}{\mu e} \sin \gamma \delta V \quad (5.13)$$

5.2.2 Reversal Direction Criteria

Examination of Equation 5.13 yielded an interesting observation. The magnitude of the position vector (r), the specific angular momentum (h), the gravitational parameter (μ), and the eccentricity (e) are all positive definite for all types of orbits. Therefore, the sign of the flight path angle determines if a lift up force increases or decreases the periapsis radius.

If a lift up force (positive impulse) is applied while the flight path angle is negative, the result of Equation 5.13 is positive and the periapsis radius will increase. A lift down force will have the same effect if the flight path angle is positive. Noting that the flight path angle is negative at the beginning of the trajectory and positive at the end of the trajectory, this result confirms the trend presented in Section 5.1. Furthermore, a switching point is clearly defined to determine which reversal direction is more beneficial. A control logic may be developed to command bank reversals through lift up when the flight path angle is negative, and reversals through lift down when it is positive.

The point at which the flight path angle changes sign from negative to positive corresponds to the point in the trajectory of closest approach to the planet. In other words,

this is the point where the magnitude of the position vector is minimum. This minimum occurs when the rate of change of the magnitude of the position vector switches from decreasing to increasing (or \dot{r} changes sign from negative to positive). Any of these parameters may be used to define the reversal direction.

Further examination of Equation 5.13 also demonstrates the effectiveness of forces in the lift direction to increase the periapsis radius. At the point where flight path angle is zero, the result of Equation 5.13 becomes zero, and lift forces will not change periapsis. Away from this point, the flight path angle and the magnitude of the position vector both increase, while the angular momentum and eccentricity change only slightly. This indicates that lift forces are most effective when applied away from the point of closest approach, but not so far that the atmospheric density becomes too low and little lift is produced.

5.2.3 Application to Simulation

To further study the bank reversal direction logic, simulations were performed to test the findings. For comparison, these simulations contained a sensitivity analysis. The sensitivity analysis was used to confirm the bank direction logic. Additional simulations contain directly applied impulses to observe the expected behavior.

With the direction logic defined, some trade studies were performed to test the effectiveness of the control law. Options for application to a nominal trajectory were also explored. This led to the selection of a final nominal trajectory for use in the complete simulation.

5.2.3.1 Gauss' Variational Equations

A derivation of a periapsis sensitivity equation begins with a set of equations representing the affect of perturbations on the orbital elements of a body in orbit about a planet. Gauss developed a general form of these equations. The two of Gauss' variational equations of interest, found on Page 488 in Reference 14, are:

$$\frac{da}{dt} = \frac{2a^2}{h} \left(e \sin fa_r + \frac{p}{r} a_s \right) \quad (5.14)$$

$$\frac{de}{dt} = \frac{1}{h} \{ p \sin fa_r + [(p+r) \cos f + re] a_s \} \quad (5.15)$$

where the perturbation acceleration is represented by components (a_r and a_s) in the body fixed RSW coordinate system. This is a body fixed reference frame composed of unit vectors in the radial direction from the center of the planet to the vehicle (R), perpendicular to the radius vector in the orbital plane in the direction of the velocity vector (S), and normal to the orbital plane completing a right hand system (W) (Reference 6). A representation is provided in Figure 5.4. This reference frame was used to develop the periapsis sensitivity equation because the variational equation calculations contained in POST are relative to the RSW frame.

The results of these equations are available in component form throughout the trajectory as standard POST output. They are represented as sensitivities to unit accelerations in each of the directions. For simplicity, time derivatives are represented by the dot notation. The available equations are:

$$\dot{a}/a_r = \frac{2a^2}{h} e \sin f \quad (5.16)$$

$$\dot{a}/a_s = \frac{2a^2 p}{hr} \quad (5.17)$$

$$\dot{e}/a_r = \frac{p}{h} \sin f \quad (5.18)$$

$$\dot{e}/a_s = \frac{1}{h} [(p+r) \cos f + re] \quad (5.19)$$

5.2.3.2 Periapsis Specific Sensitivity Equation

To make use of Equations 5.16 through 5.19, one of the equations for conic sections (Equation 5.1) is used to derive the sensitivity of the periapsis to unit accelerations:

$$r_p = a(1-e) \quad (5.20)$$

Taking the time derivative of Equation 5.20 results in:

$$\frac{dr_p}{dt} = \frac{da}{dt}(1-e) - a \frac{de}{dt} \quad (5.21)$$

which may be represented as:

$$\dot{r}_p = \dot{a}(1-e) - a\dot{e} \quad (5.22)$$

From Equation 5.22 the sensitivity of the rate of change of the periapsis radius due to a unit acceleration in each of the directions of interest may be represented by:

$$\left(\frac{\dot{r}_p}{a_r}\right) = \left(\frac{\dot{a}}{a_r}\right)(1-e) - a\left(\frac{\dot{e}}{a_r}\right) \quad (5.23)$$

and

$$\left(\frac{\dot{r}_p}{a_s}\right) = \left(\frac{\dot{a}}{a_s}\right)(1-e) - a\left(\frac{\dot{e}}{a_s}\right) \quad (5.24)$$

Finally, the sensitivity of the rate of change of the periapsis radius due to a unit acceleration in the lift up direction is calculated by simple geometry as:

$$\left(\frac{\dot{r}_p}{a_L}\right) = \left(\frac{\dot{r}_p}{a_r}\right) \cos \gamma - \left(\frac{\dot{r}_p}{a_s}\right) \sin \gamma \quad (5.25)$$

The sensitivity is easily calculated by using the results of Equations 5.16 through 5.19 in Equations 5.23 and 5.24, and those results in Equation 5.25. This represents how much the periapsis rate (m/s) is affected by an applied acceleration (m/s²).

The sign of the result of Equation 5.25 is of interest. A positive result indicates that an acceleration in the lift up direction will increase the rate of change of the periapsis location. This would lead to a larger final periapsis radius. Conversely, if the sensitivity is negative, a lift up acceleration will lead to a lower final periapsis. It was expected that the sign of Equation 5.25 would correspond to the findings presented in Section 5.2.2.

A POST subroutine was developed to calculate the sensitivity equations and some sample trajectories were simulated. An example of the sensitivities is presented in Figure 5.5. No bank reversals were performed during this trajectory so that no vertical components of lift are present to affect the sensitivities.

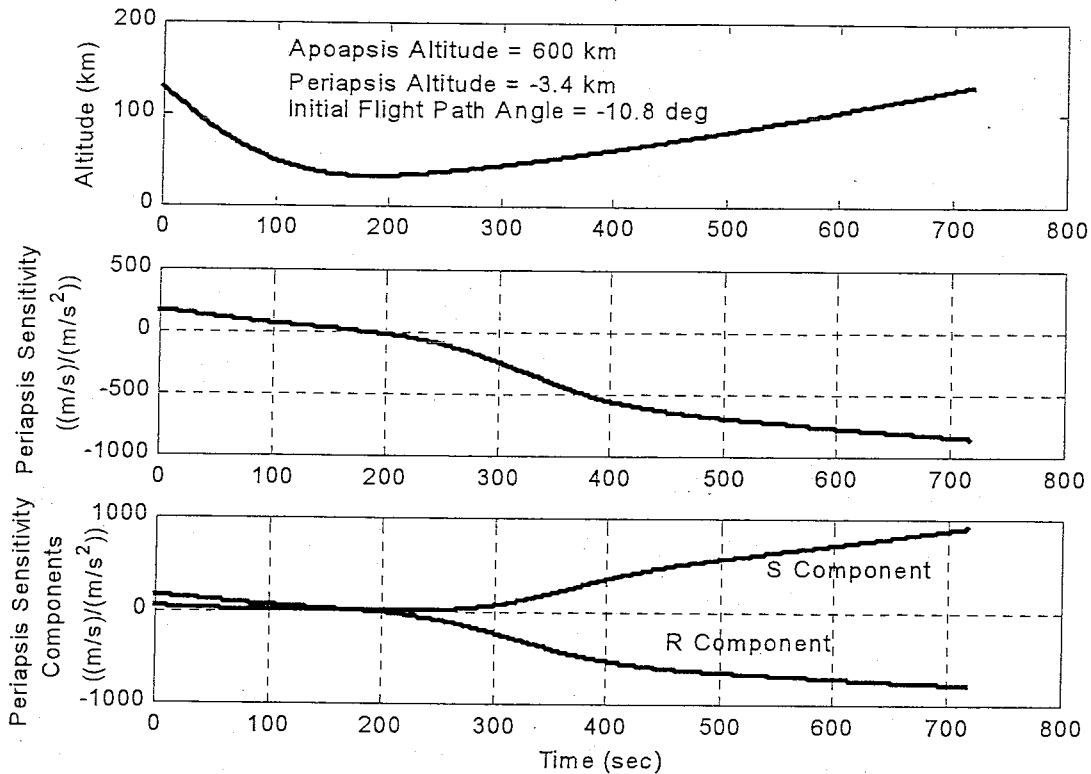


Figure 5.5: Periapsis Sensitivities for a Sample Trajectory

The total sensitivity is positive at the beginning of the trajectory, negative at the end, and changes sign exactly once. In each case, the sign of the total sensitivity switches from positive to negative precisely at the point in the trajectory of closest approach. This directly correlates to the results presented in Section 5.2.2 and confirm what was previously observed.

Figure 5.5 also illustrates how the magnitude of the sensitivity increases away from the point of closest approach. This indicates that vertical lift forces are more effective at changing the periapsis when applied farther away from this point as expected from the theory. However, atmospheric density decreases rapidly with altitude reducing the amount of lift that can be produced.

More understanding may be achieved by looking more closely at the components of the sensitivity in Figure 5.5 and Equation 5.25. At the beginning of the trajectory, both components of the sensitivity are positive, and the flight path angle is negative (approximately -10 deg). Because the cosine of any angle between ± 90 degrees is positive,

and the sine of a negative angle is always negative, each term of Equation 5.25 is positive resulting in a positive sum. After the point of closest approach the flight path angle is positive, where both the sine and cosine are positive. From Figure 5.5 it is seen that the sensitivity due to accelerations in the radial direction has become negative, while the other remains positive. Looking back at Equation 5.25 shows that the positive second term is subtracted from the negative first term resulting in a negative result.

5.2.3.3 Verification of Control Logic

To confirm the control logic, additional simulations were conducted. These simulations were performed similar to the trade study simulations discussed in Section 5.1 of this report. However, the bank dynamics model was not included and instantaneous bank reversals were performed. Impulse accelerations were added in the lift up or lift down directions at the time of bank reversal to model a finite roll. This provided greater control of the applied forces for understanding how they affected the sensitivity equations as well as an immediate response easily visible in the results.

Trajectories were calculated with bank reversals occurring at various locations and impulses added in both lift up and down directions. Throughout each trajectory the periapsis radius was calculated and monitored. This represents the osculating value of the periapsis radius, not the final value. In other words, this would be the periapsis of the resulting orbit if the atmosphere were to disappear. The final periapsis is calculated at atmospheric exit, and therefore is the periapsis of the final orbit.

The first cases tested were those with impulses applied in the proper direction for increasing the periapsis altitude. Lift up impulses were applied at bank reversals occurring while the total sensitivity is positive. An example trajectory is shown in Figure 5.6. Similarly, lift down impulses were applied at bank reversals occurring while the sensitivity is negative. An example of these trajectories is shown in Figure 5.7. Each case reaches a final orbit with the same apoapsis and inclination.

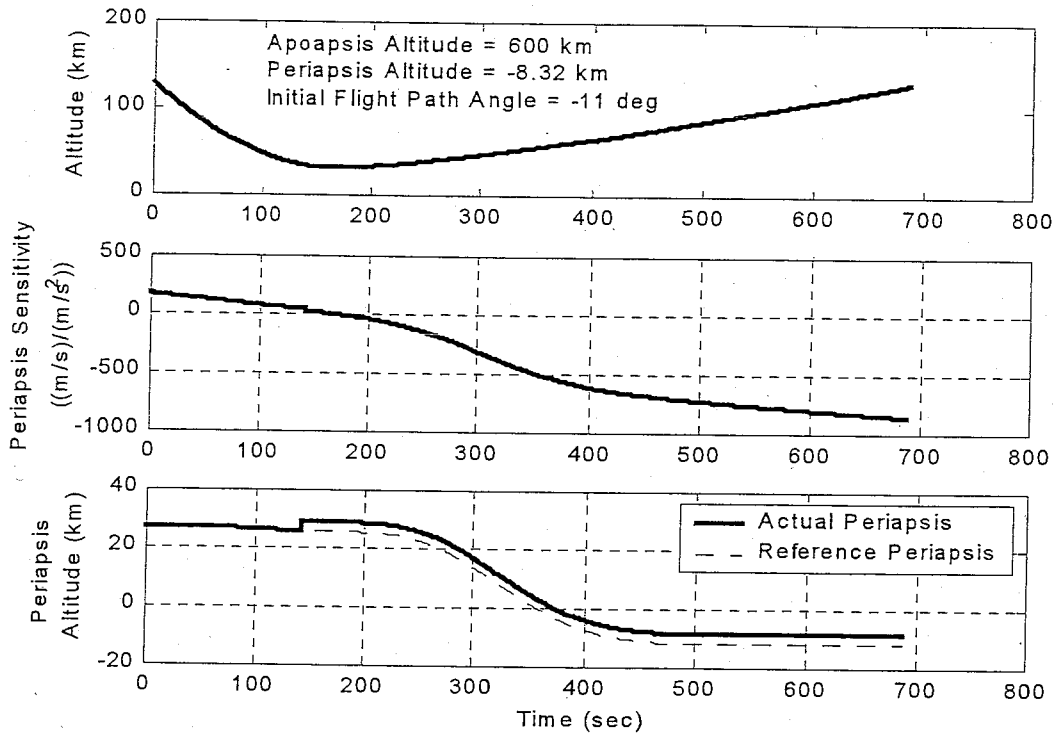


Figure 5.6: Lift Up Impulse Applied With a Positive Sensitivity

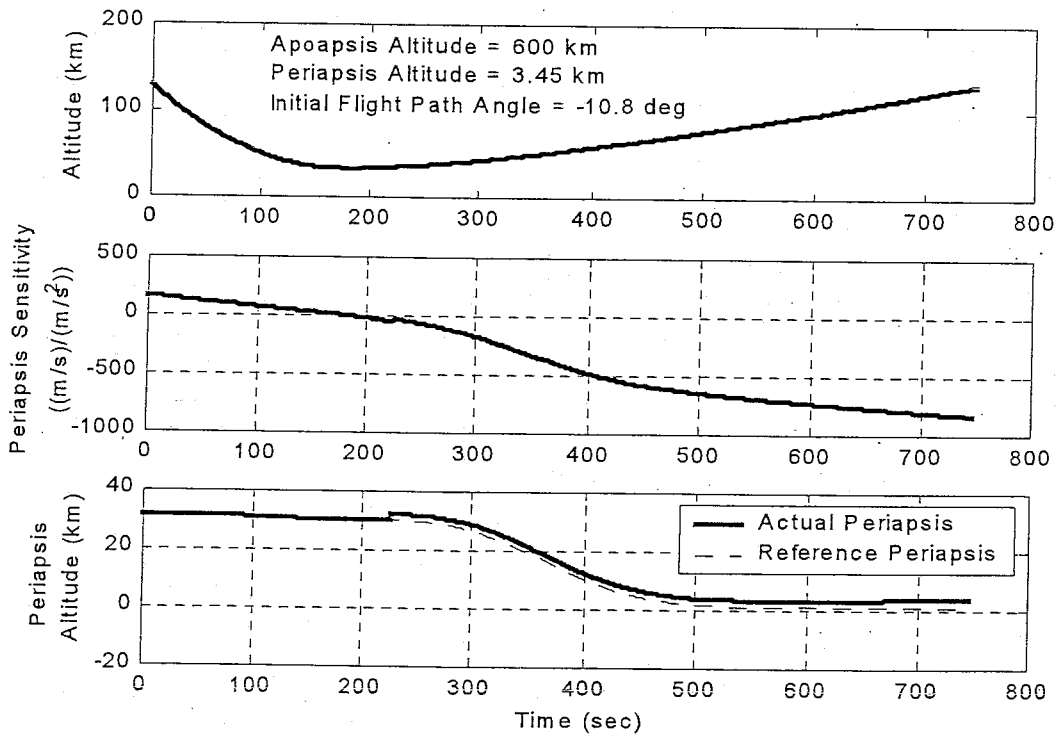


Figure 5.7: Lift Down Impulse Applied With a Negative Sensitivity

In each case, the impulse force has the effect of instantaneously increasing the osculating periapsis radius. The end result is a higher final periapsis as expected. As an additional verification, these simulations were repeated with the impulses applied in the opposite directions. Where the sensitivity is positive, a lift down impulse was applied. The results of one of these tests is provided in Figure 5.8. Also, Figure 5.9 shows a case in which a lift up impulse was applied where the sensitivity is negative.

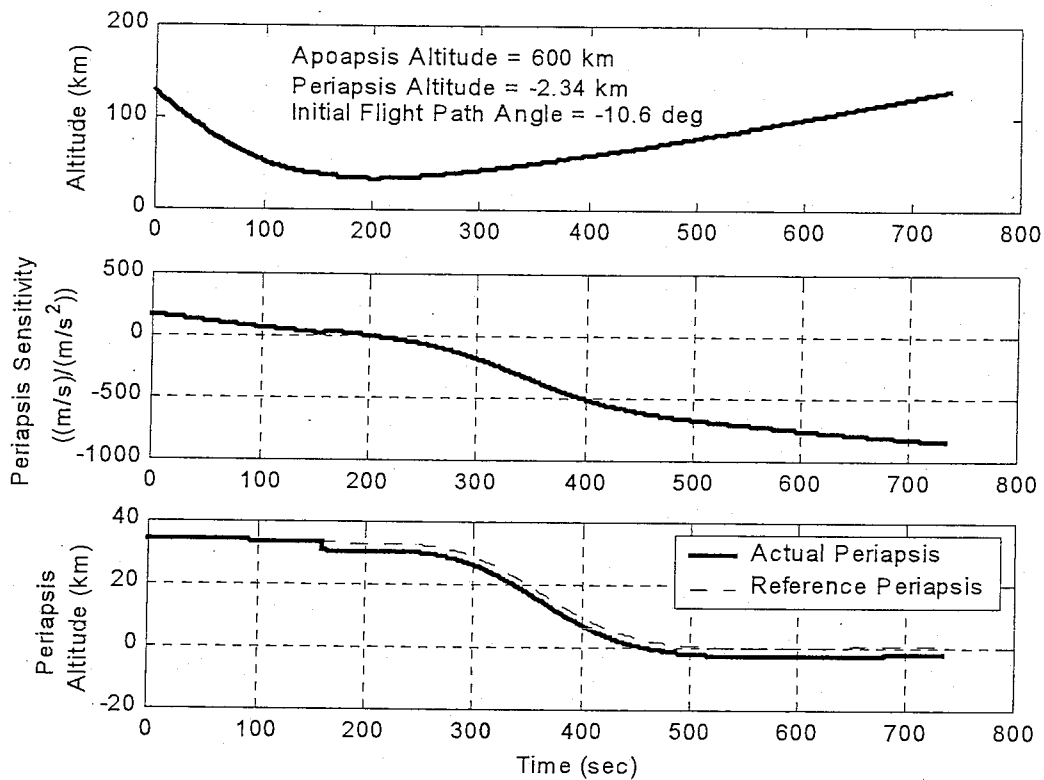


Figure 5.8: Lift Down Impulse Applied With a Positive Sensitivity

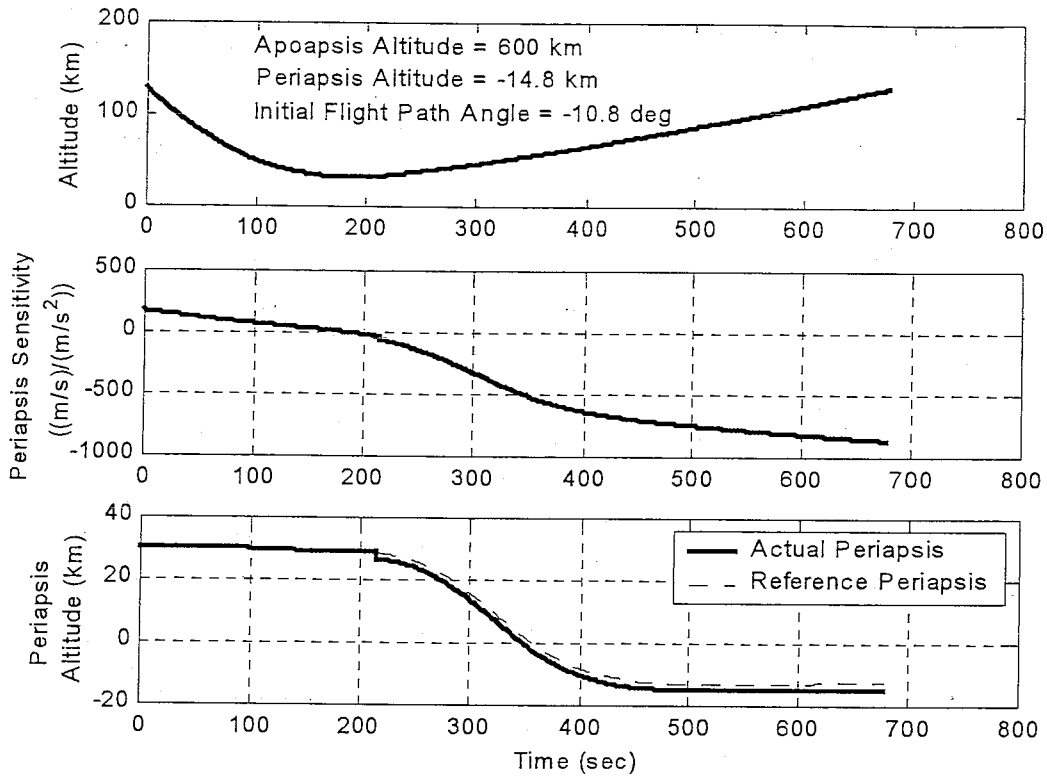


Figure 5.9: Lift Up Impulse Applied With a Negative Sensitivity

As expected, this had the inverse effect. In each case, the osculating periapsis radius decreased where the reversal occurred. This resulted in a lower final periapsis. These results confirm what was expected by the theory and better define what was observed by the sensitivity analysis and trade study. A summary of the results is presented in Table 5.1.

Table 5.1: Summary of Control Law Test Results

Impulse Direction	Time Applied	Sensitivity Sign	Final Periapsis Altitude
Lift Up	140 sec	Positive	-8.3 km
Lift Down	220 sec	Negative	3.4 km
Lift Down	160 sec	Positive	-2.3 km
Lift Up	210 sec	Negative	-14.8 km

One result of concern is the low final periapsis altitude of the first test case (Figure 5.6). The periapsis history clearly shows an increase at the point where the impulse is applied, yet the final value is lower than the third test case (Figure 5.8) in which the impulse is incorrectly applied. An explanation could come from the fact that the first test case begins with the steepest initial flight path angle of all the cases. This is required to account for the lift up impulse while targeting the same apoapsis. From Figure 5.6 it can be seen that this causes the initial periapsis to be lower. This lower starting point causes the final value to be lower despite the increase gained by the impulse.

5.2.3.4 Control Law Effectiveness

With the bank reversal direction logic defined, it is of interest to study the possible gains of employing the technique. For a spacecraft flyby trajectory of a planet with no atmosphere encountered, the periapsis altitude of the orbit after the flyby is simple the altitude at closest approach. In fact, the osculating periapsis history is simply a straight line throughout the trajectory tangent to the altitude at its minimum. For trajectories where an atmosphere is encountered, the periapsis almost always decreases from the initial value. It is possible for it to increase if lift is applied in the right direction at the proper times. This is indeed the case for the two trajectories simulated to define the entry corridor (full lift up and full lift down). How the periapsis altitude changes throughout each is shown in Figures 5.9 and 5.10 respectively.

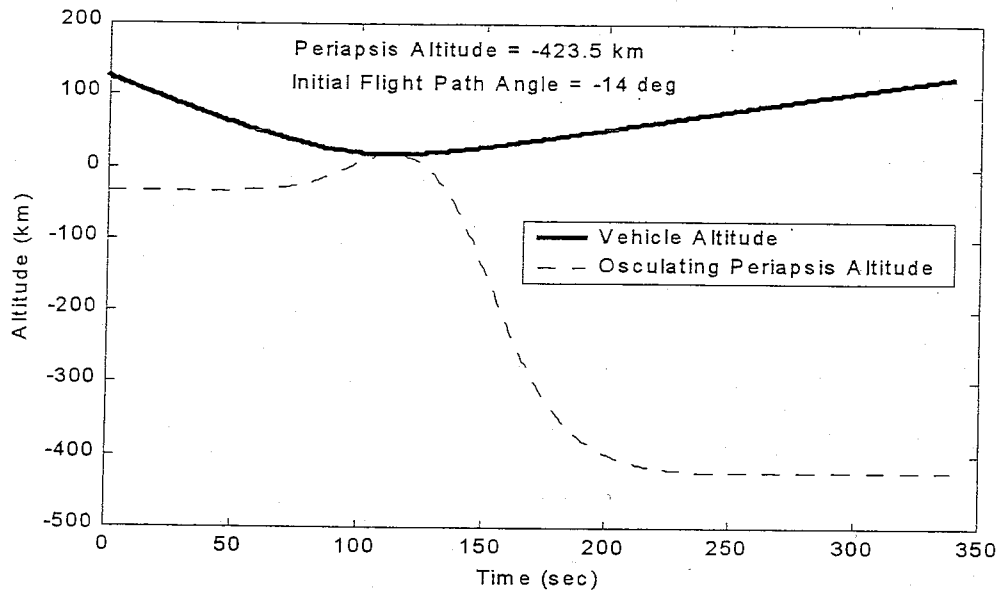


Figure 5.10: Effect of Full Lift Up Trajectory on Periapsis Altitude

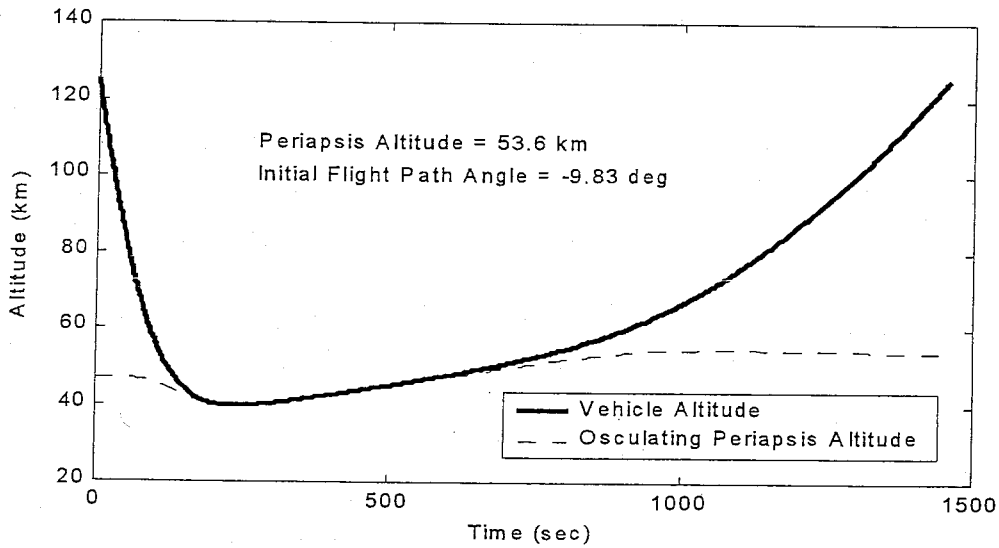


Figure 5.11: Effect of Full Lift Down Trajectory on Periapsis Altitude

Because the lift forces act in opposite directions for these two trajectories, each must have a unique initial flight path angle to target the same apoapsis. This will define the value of the initial periapsis altitude. Figure 5.10 illustrates how the full lift up trajectory begins with a steeper flight path and therefore a lower periapsis. The osculating periapsis rises while the sensitivity is positive, due to the up component of lift, until the point of closest approach. Here the periapsis altitude is equal to the actual instantaneous altitude. The

periapsis then decreases for the remainder of the trajectory because of the negative sensitivity.

The opposite behavior is apparent in Figure 5.11. A shallower initial flight path angle is required because of the lift down force, resulting in a higher initial periapsis. While the sensitivity is positive, this lift down force causes the periapsis to reduce. At the point of closest approach, the periapsis altitude is again equal to the actual altitude. The lift down force then results in increasing the periapsis because of the negative sensitivity throughout the rest of the trajectory.

Another interesting study is the examination of the best possible and worst possible control methods in terms of maximizing the periapsis. The best case would be to fly full lift up while the sensitivity is positive, and switch to full lift down while the sensitivity is negative. This would have the effect of continuously increase the periapsis. Figure 5.12 represents this trajectory. The opposite control logic would then be the worst case. A trajectory using the opposite logic is summarized by Figure 5.13.

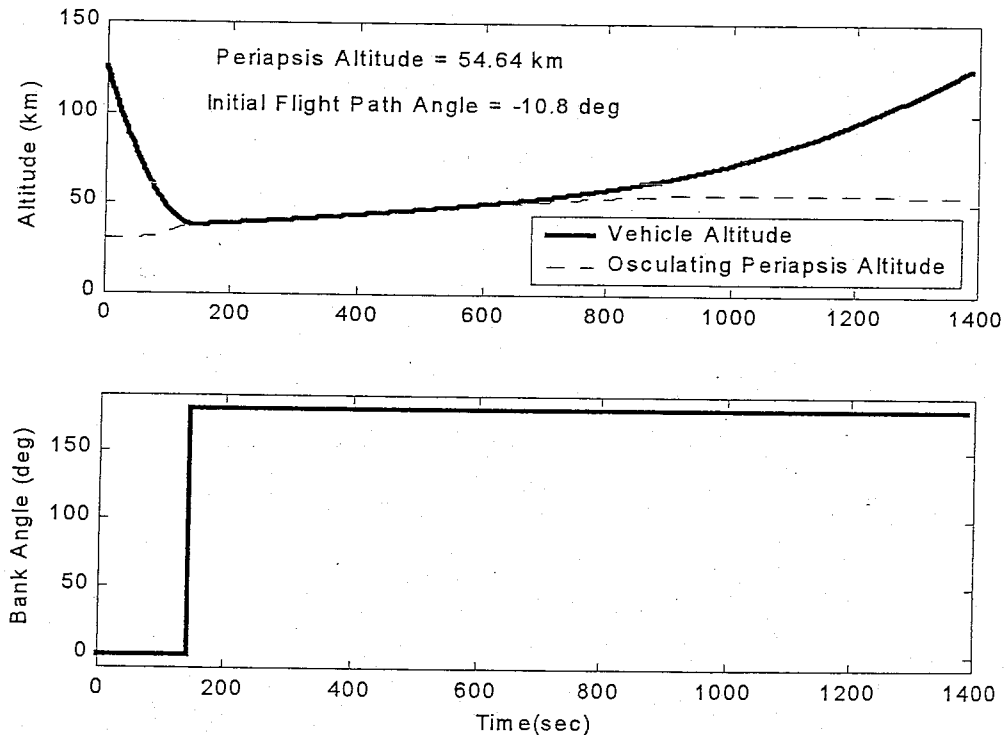


Figure 5.12: Effect of Best Case Lift Control on Periapsis Altitude

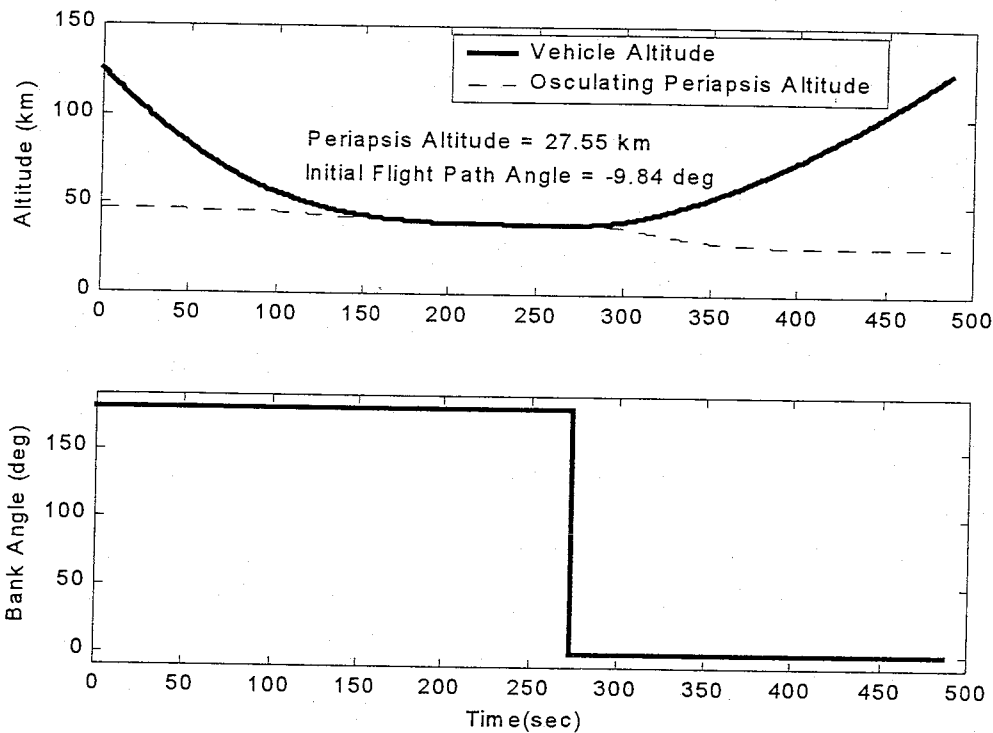


Figure 5.13: Effect of Worst Case Lift Control on Periapsis Altitude

As expected, the periapsis rises continuously throughout the whole of the best case trajectory. In addition, the final periapsis is the highest of all the example test cases. It is not significantly higher, however, than the full lift down trajectory. The shallow initial flight path of the lift down trajectory creates the advantage of a much higher initial periapsis, so the final value is large despite the loss. The advantage of the best case scenario over the full lift up trajectory is significant. These two observations suggest that the final periapsis is more sensitive to the lift direction during the final segment of the trajectory than the initial portion. This can also be seen in the sensitivity histories presented in Section 5.2.3.2. In every case, the magnitude of the sensitivity is much larger toward the end of the trajectory than at the beginning.

The worse case trajectory affirms the trend. The periapsis altitude continuously decreases through the trajectory. The final value is low, though not as low as that of the full lift up trajectory. This is still considered the worst case in terms of bank profile relative to the sensitivity, even though it did not produce the lowest periapsis. A similar argument may be made that the steep initial flight path of the lift up trajectory causes a disadvantage by

resulting in a much lower initial periapsis altitude. This is similar to the behavior observed in Section 5.2.3.4.

Another scenario was examined to design the nominal bank angle to increase the periapsis altitude at all times, not just during reversals. For inclination control, only the out of plane force component of lift is important. This leaves two possible bank angles that provide the same out of plane component. For example 60 degrees and 120 degrees bank angle would both have the same affect on inclination, but would yield completely different results in apoapsis and periapsis. A nominal trajectory was devised that targets the proper apoapsis while fixing the bank angle such that the vertical component of lift works with the sensitivity to further increase the periapsis. In other words, rather than bank reversals always occurring between ± 60 degrees bank angle, a nominal bank angle magnitude is chosen as ± 60 or ± 120 degrees for different portions of the trajectory depending on which provides a more beneficial vertical component while not affecting the out of plane component.

Preliminary studies of this method show significant advantages over the ± 90 degree nominal bank angle trajectory. A trajectory was devised to begin with a 60 degree nominal bank angle. The first reversal occurs just prior to the point of closest approach. To take advantage of the sensitivity change, the reversal is commanded to continue until reaching a bank angle of -120 degrees. For the remainder of the trajectory, all reversals occurred between ± 120 degrees. This trajectory is represented by Figure 5.14.

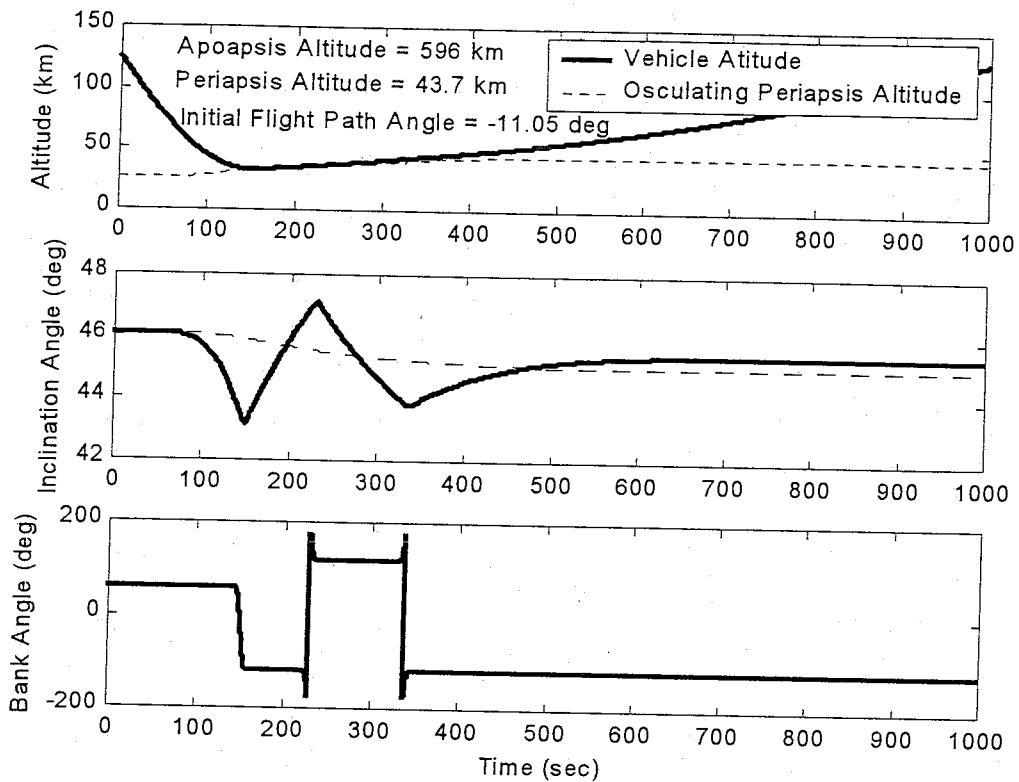


Figure 5.14: Trajectory With Nominal Vertical Lift Component

The much higher periapsis altitude achieved is possible by applying vertical components of lift throughout the entire trajectory. This preliminary result is encouraging for future applications of the control logic. However, this method appears to exhibit some of the sensitivity to initial conditions similar to those for the best case scenario presented in Figure 5.12. A discussion of this phenomenon is provided in Section 5.2.3.5. This is another reason why only the ± 90 degree nominal bank angle trajectory was examined fully in this study.

Notice that the osculating periapsis is always equal to the actual altitude at the point of closest approach in each example scenario. This is similar to the behavior expected from a planetary flyby in which no atmosphere is encountered.

Overall, these results confirm the control logic defined by the theory. A summary of these results is provided in Table 5.2. Additionally, a case with full out of plane force is included for comparison. The results are taken from those presented in Section 4.2.1 to examine the effect of no vertical component of lift being present. Three of the test cases

resulted in final periapsis altitudes higher than the point of closest approach. This shows that the atmosphere can be used to increase the periapsis altitude over the initial value set by the approach conditions. An illustration of the results is presented in Figure 5.15.

Table 5.2: Summary of Control Law Example Scenarios

Bank Scenario	Initial Flight Path Angle	Final Periapsis Altitude
Full Lift Up	-13.98 deg	-423 km
Full Lift Down	-9.83 deg	53 km
Best Case	-10.79 deg	55 km
Worst Case	-9.84 deg	28 km
60/120 Bank Case	-11.05 deg	44 km
Full Out of Plane Force	-10.79 deg	-5 km

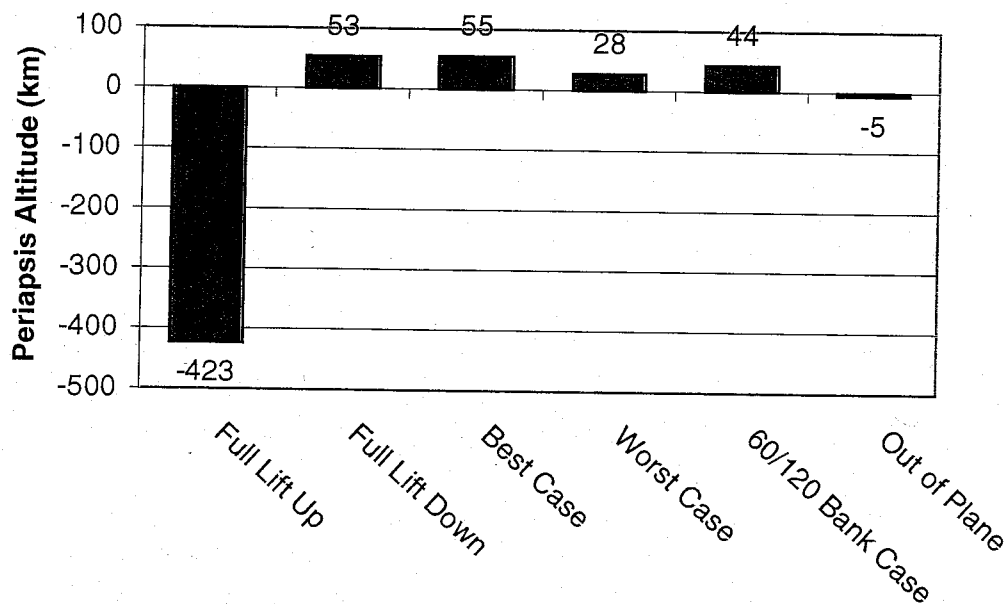


Figure 5.15: Results of Control Law Example Scenarios

5.2.3.5 Disadvantages of Directly Applied Control Law

Ideally, an actual mission would be designed to fly the best case trajectory for maximum benefit. Several difficulties arise if this logic were to be directly applied to a guidance algorithm. The most noticeable is that lift up and lift down only orientations provide no out of plane force for inclination control. Existing guidance algorithms limit the bank angle range so that lift up and down commands are never issued to retain inclination control (Reference 5). A guidance algorithm trying to follow this logic would lose inclination control when targeting apoapsis, and lose apoapsis control when targeting inclination.

Another disadvantage is that the vertical component of lift cannot be adjusted to account for off nominal conditions such as density variations. It was found that the trajectory is extremely sensitive to the initial flight path angle, so much so, that accounting for uncertainties becomes impossible. For example, a variation of just 0.01 degrees can mean the difference between entering too steep and impacting the surface, and entering shallow enough to exceed the target apoapsis by 4,000 kilometers. This was true for both the best case scenario and the 60/120 degree bank angle cases discussed in the previous section.

To illustrate this behavior, a series of trajectories, following the best case logic, were simulated for various initial flight path angles. The results are presented in Figure 5.16. From this, the sensitivity of the final apoapsis altitude to flight path angle can be seen. It is clear that any error in the arrival state could have drastic effects.

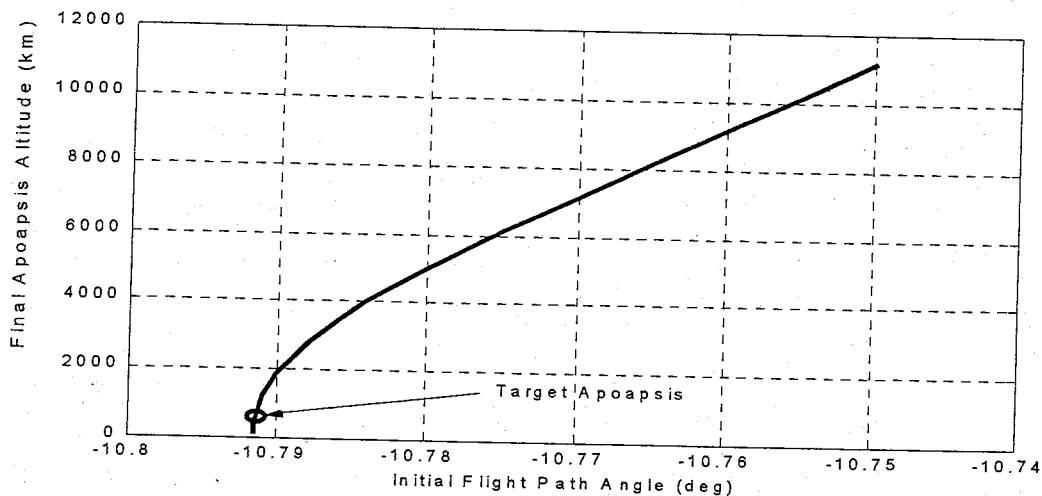


Figure 5.16: Sensitivity of Final Apoapsis to Initial Flight Path Angle

Because of these difficulties, using the example scenarios presented in Section 5.2.3.4 as a basis for a guidance algorithm is not feasible. However, applying the knowledge gained to a roll reversal algorithm is uncomplicated and advantageous. The periapsis sensitivity may be considered when choosing nominal trajectories and bank commands as well as commanding bank reversal directions.

5.3 Application to Vehicle Controller

Applying this control logic to a bank reversal guidance algorithm requires only minor modifications. Whenever a reversal command is given, a check of the bank direction criteria must be made, and a direction must be commanded. As mentioned, because a 90 degree nominal bank angle was chosen for this study, all reversals require 180 degrees of movement. This eliminates the concern that one direction might require motion through a greater angular distance than the other direction.

The selection of a direction criteria presents many options, because the sensitivity changes sign at a point when many parameters have discernible values. Depending on available spacecraft instruments, different switching criteria may be used. For this study it is convenient to make use of the fact that the sensitivity changes sign at the same point as the flight path angle, which could be used if the vehicle orientation is accurately known from onboard instruments such as gyros. This is also the same point where the rate of change of the position vector magnitude changes sign. This criterion could be used for vehicles with radar altimeters if the planet topography is known.

5.3.1 Final Inclination Boundary Definition

With more about the bank control defined, it becomes possible to define the inclination boundaries to be included in the bank reversal guidance algorithm. The simulations used for this were modified trajectories similar to those discussed in Section 4.2. The simulation was the same in that the POST targeting routine was used to search for the initial azimuth and flight path angles to target apoapsis and inclination. The first inclination deviation and ratios were also included as control variables. The initial values were varied manually to study different scenarios for maximizing the periapsis. Additionally, the bank

dynamics model was included, as well as the control law for commanding bank directions at each reversal.

For the single reversal case, there is a unique solution for a given initial state. Therefore, no manual iterations could be made. The resulting trajectory is represented by Figure 5.17.

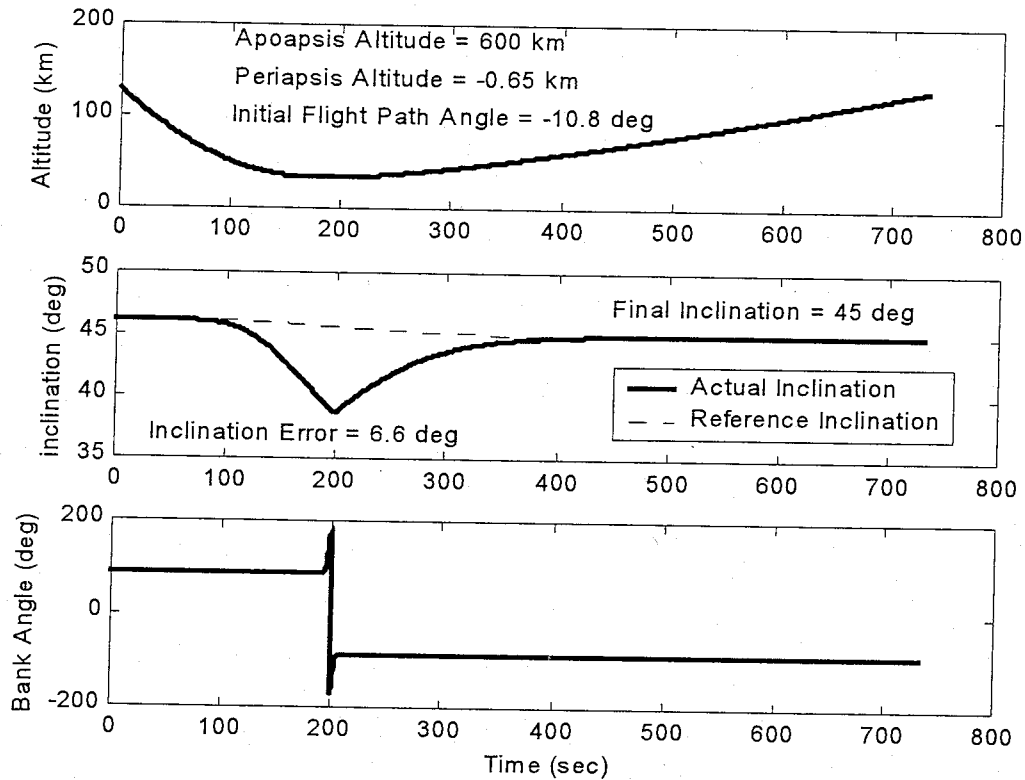


Figure 5.17: Single Bank Reversal Nominal Trajectory

The bank reversal occurs just after the point of closest approach, and a lift down reversal is commanded. So near to the logic switching point, the periapsis sensitivity magnitude is small and the reversal has only a slight affect on the final periapsis altitude.

The two reversal scenario provides more flexibility in selecting the reversal criteria. There is no unique solution because many combinations of inclination deviations and deviation ratios provide satisfactory results. The initial conditions set in the POST targeting routine may be varied until a trajectory with a high periapsis and steadily reducing inclination deviations is found. It is desired that the maximum deviation from the reference inclination is convergent throughout the trajectory. A sample trajectory is represented in Figure 5.18.

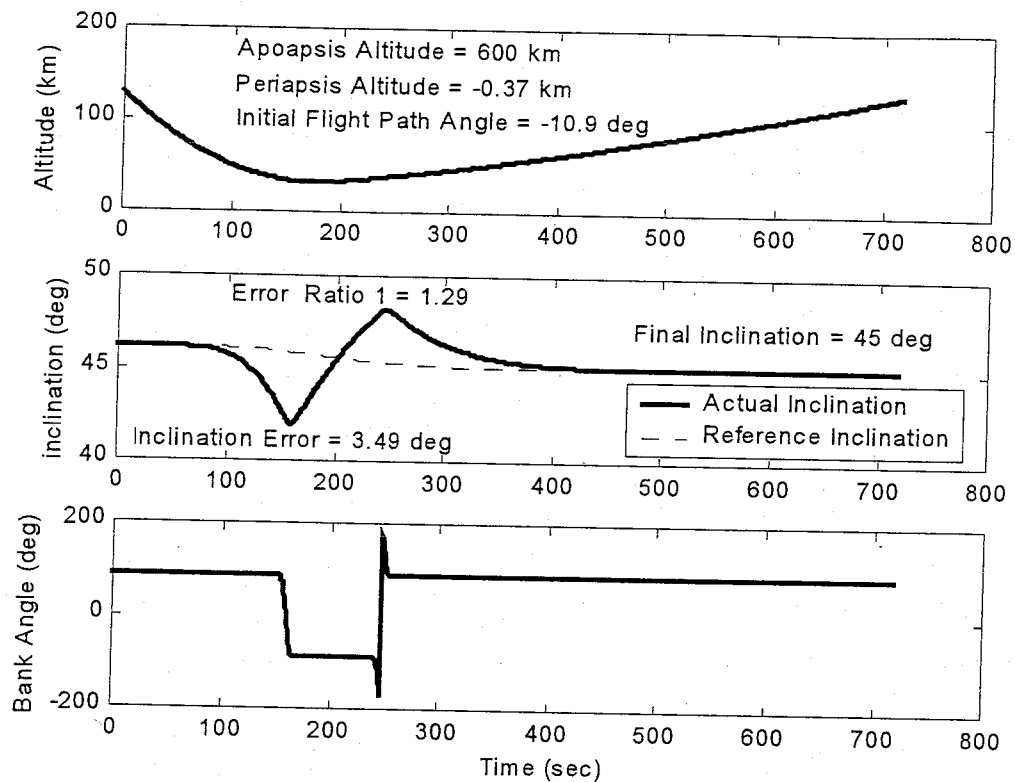


Figure 5.18: Double Bank Reversal Nominal Trajectory

The final periapsis of this trajectory is slightly higher than that of the previous trajectory. This is likely due to the additional opportunity to apply vertical lift components through the second reversal in combination with the reversals occurring farther from the logic switching point where the sensitivity magnitudes are larger.

The three reversal scenario yielded much better results. The greater flexibility in choosing reversal criteria let to more opportunities to employ the advantages of the sensitivities. This trajectory is represented by Figure 5.19.

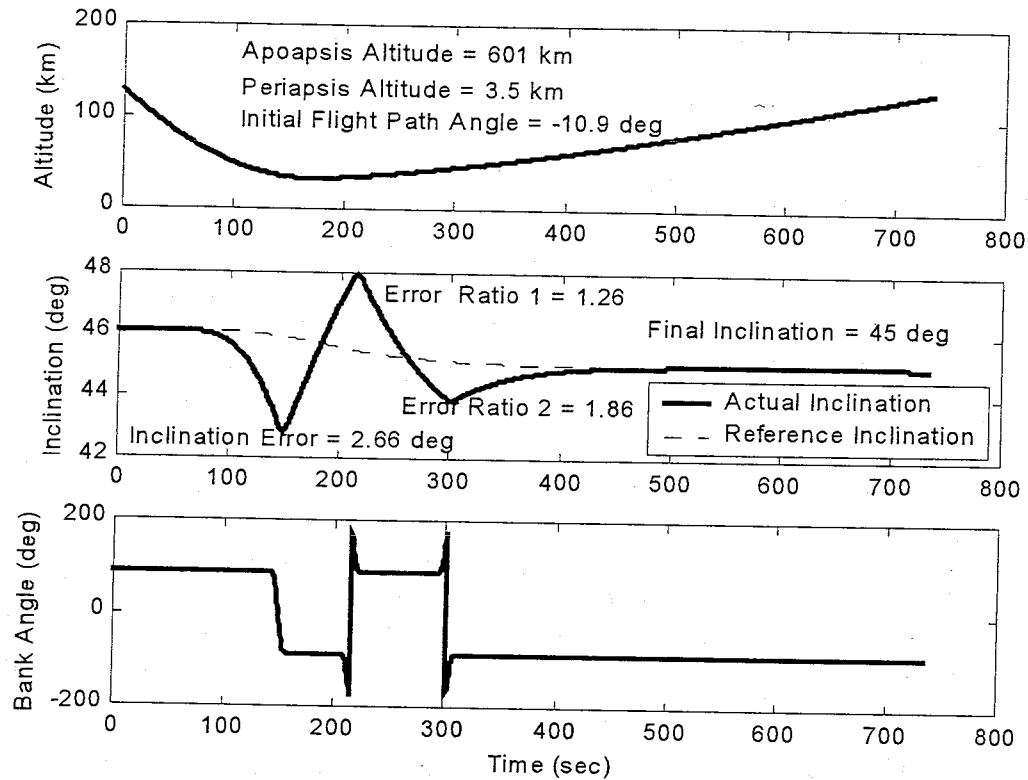


Figure 5.19: Triple Bank Reversal Nominal Trajectory

The three reversal scenario resulted in the highest periapsis of all the cases examined due to the additional opportunities to apply vertical lift components for each additional reversal and the greater sensitivity magnitudes at each reversal. This scenario was chosen for the nominal trajectory because of the periapsis advantage, and the well defined reversal points convergent toward the nominal.

The points at which each of the reversals took place were recorded. From these points, it is possible to define boundaries for an inclination deadband. The boundaries were defined by fitting polynomials through the reversal points. The inclination deviation ratios were chosen by iteration so that the boundary polynomials would be smooth and symmetrically convergent to the target inclination angle. It is convenient to define these inclination polynomials in terms of orbital energy because it is an available parameter within the guidance algorithm and less susceptible to off nominal conditions than other parameters (such as time). The chosen equations are as follows:

$$\text{Upper boundary:} \quad i = 2.6032\hat{\varepsilon}^2 + 7.4337\hat{\varepsilon} + 50.3414 \quad (5.26)$$

$$\text{Lower boundary:} \quad i = -2.0507\hat{\varepsilon}^2 - 5.8559\hat{\varepsilon} + 40.7711 \quad (5.27)$$

where the inclination result is in degrees and the nondimensional parameter is found by normalizing orbital energy as follows:

$$\hat{\varepsilon} = 2 \frac{R}{\mu} \varepsilon \quad (5.28)$$

These polynomials become part of the guidance algorithm and determine when a bank reversal command is issued.

5.3.2 Application to Nominal Simulation

Development of the inclination boundary polynomials and the nominal trajectory were performed simultaneously in an iterative process. The end result is the definition of an entry state (flight path angle and azimuth angle), bank reversal conditions (inclination deadband), and reversal direction logic that combine to result in the target final state. A robust nominal trajectory is desired so that off nominal conditions and entry state dispersions can be corrected by the guidance algorithm. Avoiding control issues such as those discussed in Section 5.2.3.5 is important. In addition, a trajectory with bank reversals in both directions was desired to demonstrate the reversal control law. The chosen nominal trajectory is shown in Figure 5.20.

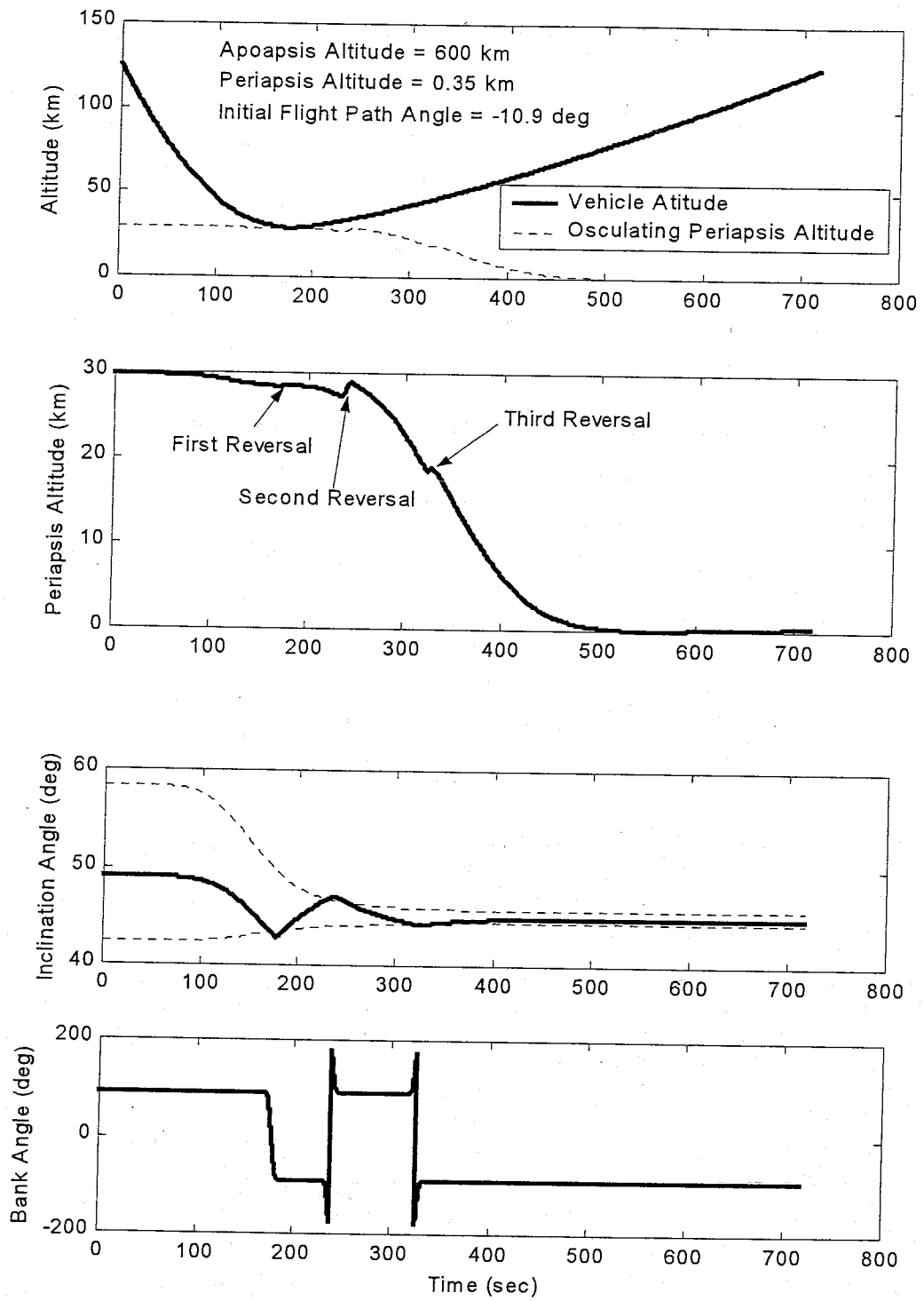


Figure 5.20: Nominal Trajectory With Bank Reversal Control Law

Examining the inclination and bank angle plots demonstrates where bank reversals are commanded and in which direction they are performed. It can be seen how one reversal occurs through lift up before the point of closest approach, and two occur lift down after the point of closest approach. Two reversals occurring later in the trajectory take advantage of the increased effectiveness to increase the periapsis due to the larger sensitivity magnitude. Also noticeable is the affect of each reversal on the osculating periapsis altitude. The osculating periapsis steadily increases through the duration of each reversal. This represents the expected and desired behavior.

To test the feasibility of applying this nominal trajectory to an actual mission, some common mission constraints were considered. For the nominal trajectory presented in Figure 5.20, the maximum sensed acceleration calculated in the simulation is slightly over two times the acceleration due to gravity at sea level on Earth (2 g's). It is believed that this is an acceptable level for most all Mars mission types.

In this study it is assumed that the aerodynamic heat rate and total heating of the nominal trajectory are acceptable given currently available thermal protection materials. Often the thermal protection system is designed to withstand the heat loads produced by the design trajectory. This is considered to be true for this study.

5.4 Application to Apollo Algorithm

To demonstrate how these findings may be applied to an actual mission, they were included in an existing aerocapture terminal point guidance algorithm (Reference 5). This is a proven, robust guidance routine based on the Apollo entry guidance algorithm. With a complete guidance routine included in the simulation, POST targeting is not utilized. Consequently, simulation parameters are no longer varied to reach specified targets, and POST is used only to integrate the equations of motion to determine the trajectory. The guidance algorithm is used for adjusting the control parameter to meet the desired result.

The algorithm applies the optimum control methods described in Reference 15 for fixed terminal time continuous systems. The objective is to define a control function, $u(t)$, for a set of non-linear differential equations described by (from Reference 15):

$$\dot{x} = f[x(t), u(t), t] \quad (5.29)$$

where the initial conditions, $x(t_0)$, are known.

The control function must satisfy Equation 5.29 while being used to maximize or minimize a performance index given by:

$$J = \phi[x(t_f), t_f] + \int_{t_0}^{t_f} L[x(t), u(t), t] dt \quad (5.30)$$

where L is the Lagrangian of the system.

In this case, the objective is to minimize the performance index defined as the ΔV required to circularize the orbit. The minimum of the performance index is found by considering the differential of Equation 5.30 due to differential changes in the control function. The minimum occurs where this differential is zero.

A set of influence coefficients, $\lambda(t)$, are introduced for convenience. There is an influence coefficient corresponding to each term of the state vector, $x(t)$. These represent the affect of each component of the state on the performance index. They are defined to eliminate terms from the differential of the performance index such that the result is zero. The system is then simplified to a two-point boundary-value problem in terms of the influence coefficients. A detailed description of the theory can be found in Reference 15.

The influence coefficients are found by integrating backward along the nominal trajectory as a reference (Section 5.3.2). The equations for aerocapture problems, from Reference 5, are as follows:

$$\frac{d\lambda_s}{dt} = 0 \quad (5.31)$$

$$\begin{aligned} \frac{d\lambda_v}{dt} = & -\cos \gamma(t) \lambda_s(t) + \left(\frac{2D(t)}{mV(t)} \right) \lambda_v(t) \\ & + \left[\frac{L(t) \cos \phi(t)}{mV^2(t)} + \left(\frac{1}{r_e + h(t)} + \frac{g}{V^2(t)} \right) \cos \gamma(t) \right] \lambda_\gamma(t) - \sin \gamma(t) \lambda_h(t) \end{aligned} \quad (5.32)$$

$$\begin{aligned} \frac{d\lambda_\gamma}{dt} = & V(t) \sin \gamma(t) \lambda_s(t) + g \cos \gamma(t) \lambda_v(t) \\ & + \left[\left(\frac{V(t)}{r_e + h(t)} - \frac{g}{V(t)} \right) \sin \gamma(t) \right] \lambda_\gamma(t) - V(t) \cos \gamma(t) \lambda_h(t) \end{aligned} \quad (5.33)$$

$$\frac{d\lambda_h}{dt} = \left(\frac{-D(t)}{mh_s(t)} \right) \lambda_v(t) + \left(\frac{L(t)\cos\phi(t)}{mh_s(t)V(t)} + \frac{V(t)\cos\gamma(t)}{(r_e + h(t))^2} \right) \lambda_\gamma(t) \quad (5.34)$$

$$\frac{d\lambda_u}{dt} = -\lambda_\gamma(t) \frac{L(t)}{mV(t)} \quad (5.35)$$

A set of feedback control gains is defined to simplify the control function. The gains are function of the influence coefficients and some reference parameters. They are calculated by the following equations from Reference 5:

$$G_1 = -\frac{mh_s(\varepsilon)\lambda_h(\varepsilon)}{D^*(\varepsilon)} \quad (5.36)$$

$$G_2 = \frac{\lambda_\gamma(\varepsilon)}{V^* \cos\gamma^*(\varepsilon)} \quad (5.37)$$

$$G_3 = \lambda_v(\varepsilon) \quad (5.38)$$

$$G_4 = \lambda_u(\varepsilon) \quad (5.39)$$

These gains, along with trajectory specific parameters, are then included in the algorithm. Throughout the simulation, bank angle commands are calculated by the algorithm to correct for deviations in the actual state from the nominal state. Deviations from nominal of the velocity, altitude rate, and drag acceleration are considered. The bank angle control command is then calculated by the following equation from Reference 5:

$$\cos\phi_{cm} = \cos\phi^* - \frac{K}{G_4} \left\{ G_3 [V(\varepsilon) - V^*(\varepsilon)] + G_2 [\dot{h}(\varepsilon) - \dot{h}^*(\varepsilon)] + G_1 \left[\frac{D(\varepsilon)}{m} - \frac{D^*(\varepsilon)}{m} \right] \right\} \quad (5.40)$$

where the starred terms represent values from the reference nominal trajectory, and K is called an overcontrol factor.

The overcontrol factor is available to the user for manually adjusting the gains. This is a multiple on all of the gains to increase or decrease the magnitude of the control command. This provides a means for tuning the algorithm for optimal performance for the specific problem.

A detailed description of the algorithm derivation may be found in Reference 5. For this study, it has been assumed that the Apollo algorithm receives perfect navigation information since the exact vehicle position and velocity are provided. For an actual application, this will not be the case and errors in the final state will be slightly greater.

The algorithm controls the bank angle while all other parameters are simulated by POST. A bank angle command and direction are output from the algorithm and passed to the bank dynamics routine. The bank angle is then provided to the rest of the simulation. The algorithm was modified by including the inclination deadband boundary polynomials to be used as bank reversal criteria. The bank direction control logic was also included for determining the command bank direction. A flow diagram on the controller is included in Appendix B.

The final result is a simulation intended to model an actual mission. Starting from a given initial state, the equations of motion are integrated until atmospheric exit. Any deviation from the nominal atmosphere or initial conditions must be corrected by the guidance algorithm to achieve the desired final state.

6 Results

With the complete simulation assembled a series of trajectories were calculated for various conditions. By changing certain parameters, off nominal scenarios can be examined. The intent is to test the robustness of the guidance and control laws for situations that might be encountered during an actual mission.

The first simulation performed is simply the nominal case. It is important to be sure that the guidance routine follows the nominal trajectory to check for any implementation errors which might cause a deviation. Simulation results are presented in Figure 6.1.

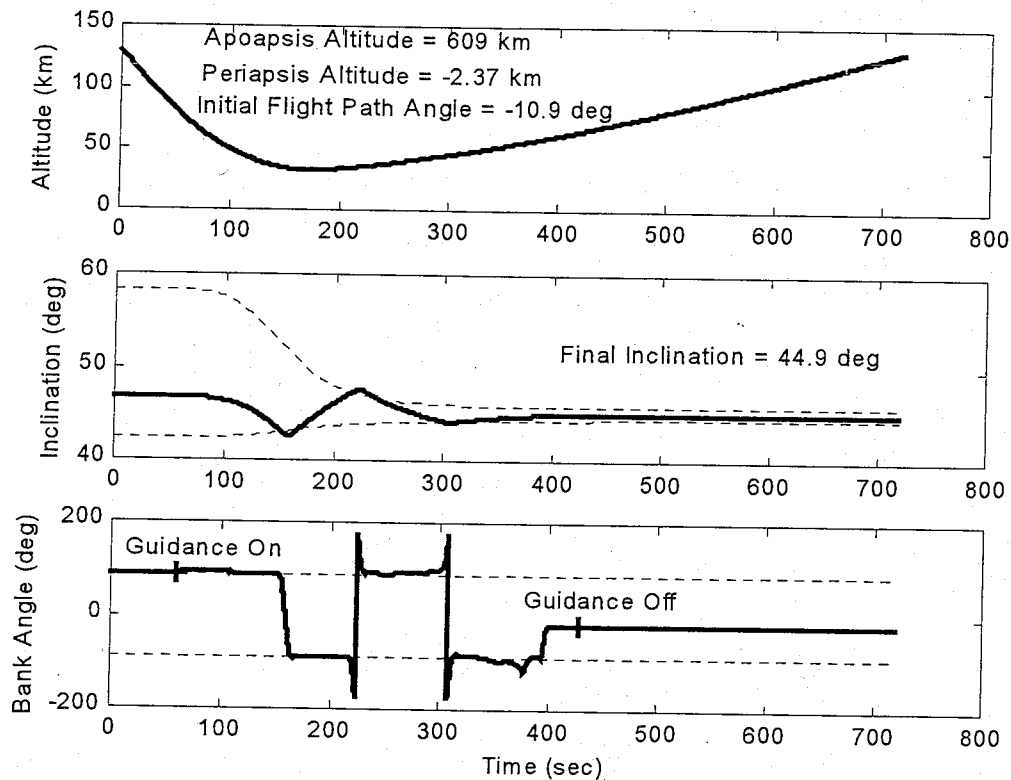


Figure 6.1: Full Simulation with Nominal Conditions

The simulation with all nominal conditions does closely follow the POST targeted nominal trajectory. The only exception is some irregular bank angle commands toward atmospheric exit. This results from the guidance algorithm calculating commands where there is too little control authority left due to the low density atmosphere.

A related result is seen by the lift up commands occurring near atmospheric exit (where the bank angle becomes zero). This is an undesirable trend since lift down forces increase the periapsis in this portion of the trajectory. When the nominal trajectory is integrated to calculate the influence coefficients, the low density in this region results in little control authority and small influence coefficients. As a result, the control gains approach zero. This causes the lift up commands to be issued. They have very little affect, however, since the aerodynamic forces are so small by this time.

Also illustrated are the times active guidance is initiated and terminated. The Apollo algorithm is used to calculate and issue bank commands only when the sensed acceleration on the vehicle is greater than 0.03 g's. This prevents ineffective commands from being issued when the vehicle is not in the atmosphere.

Next, several off nominal cases were simulated. Because it was previously observed that the trajectory is particularly sensitive to the initial flight path angle, this parameter was varied ± 0.5 degrees. Modern navigation systems are capable of finding the entry state with much higher degrees of accuracy; therefore this represents a significant error. Each of these cases is presented in Figure 6.2 and Figure 6.3.

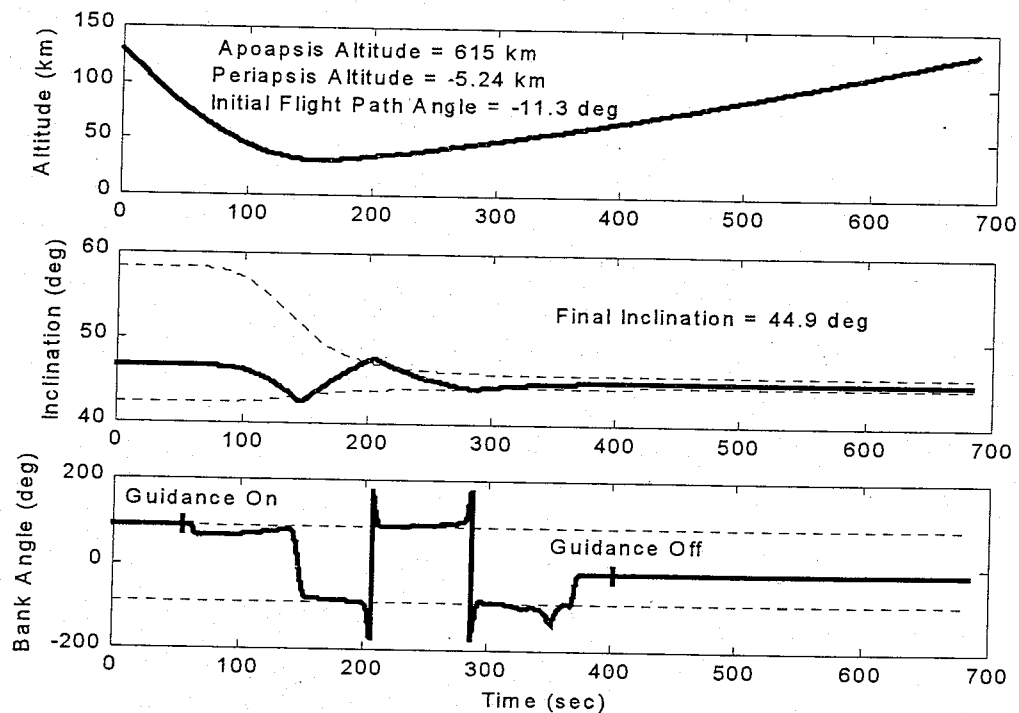


Figure 6.2: Full Simulation with -0.5 Degree Flight Path Angle Error

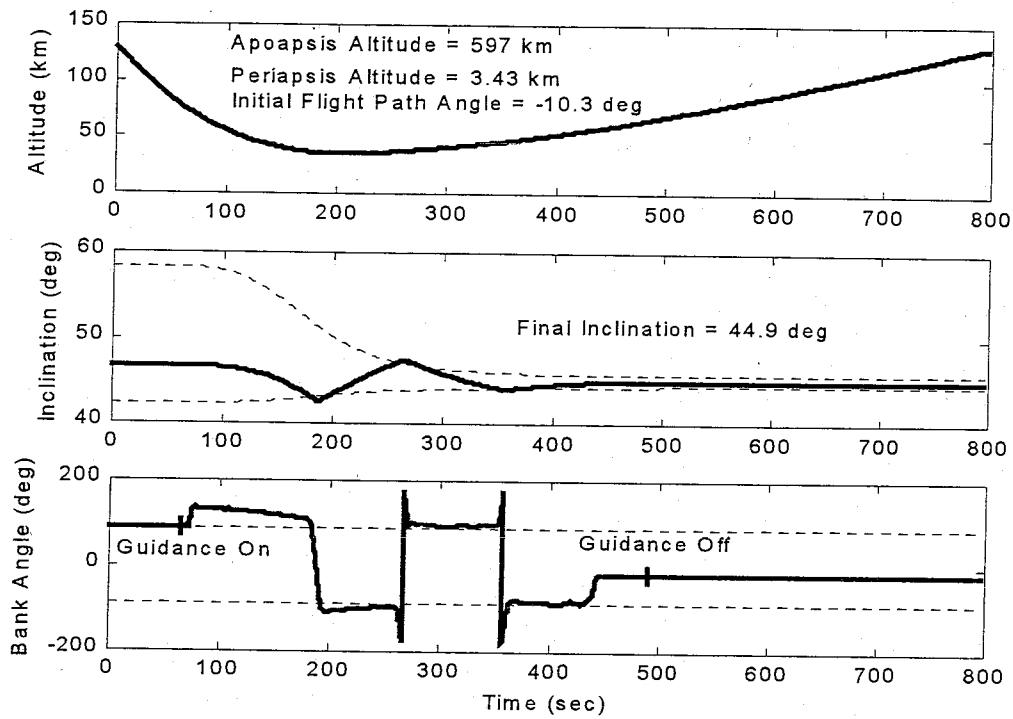


Figure 6.3: Full Simulation with +0.5 Degree Flight Path Angle Error

In each of the off nominal simulations, the target conditions were met with acceptable accuracy. How the error is compensated is easily visible in the bank angle histories. In Figure 6.2, for example, the bank angle is first decreased from nominal. This creates a lift up component to counter the steep flight path. As the vehicle converges back toward the nominal trajectory, the bank angle returns toward the nominal with the decreasing error. The large initial bank angle command is representative of the reduced effectiveness at the beginning of the trajectory where the atmosphere is still thin. As the vehicle enters more dense regions, the bank angle command may be reduced toward nominal while still producing the same vertical lift component. Similar behavior may be observed in Figure 6.3, where a lift down component of lift, created by the increased bank angle magnitude, drives the trajectory steeper to counter the shallow initial state.

It is also possible that there could be errors in the initial azimuth angle of the vehicle. This would lead to inclination errors. This parameter was also varied ± 0.5 degrees representing a significantly large error. The representations of the resulting simulations are presented in Figure 6.4 and Figure 6.5.

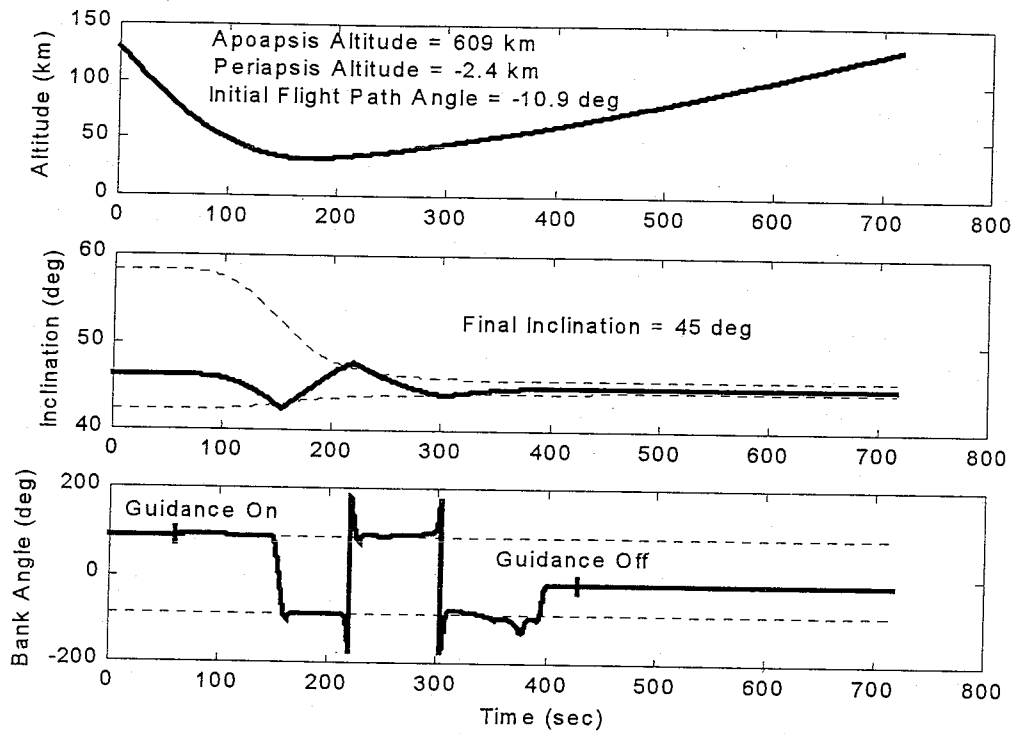


Figure 6.4: Full Simulation with +0.5 Degree Azimuth Angle Error

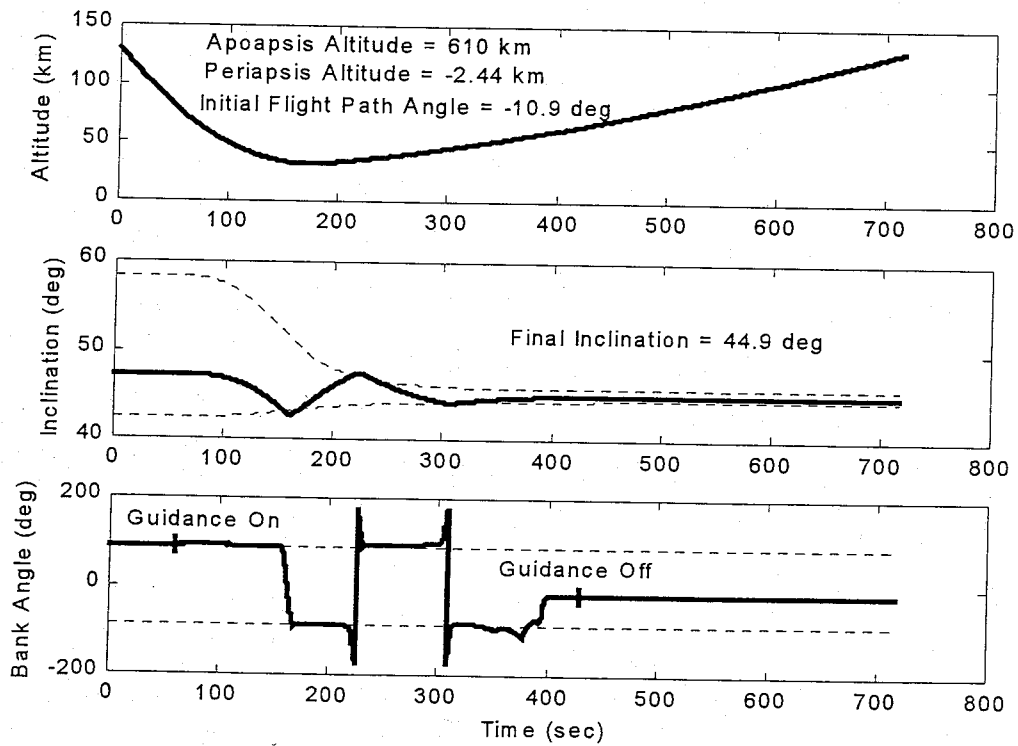


Figure 6.5: Full Simulation with -0.5 Degree Azimuth Angle Error

In both cases the inclination boundaries successfully commanded reversals to drive the inclination angle toward the desired final value. The reversals occurring at different time had effects on other parameters causing errors in the apoapsis altitude. The guidance algorithm issued bank angle commands to overcome these errors. This can be seen as the bank angle departs from nominal.

Another potential source for error exists in the initial velocity. While it was found that decreases in the velocity could be easily corrected by commanding bank angles for lift up forces, increases in velocity were not as easily overcome. Full lift down commands were not as effective at removing the excess energy. To simulate these scenarios, an initial velocity error of ± 20 m/s was introduced. The resulting trajectories are shown in Figure 6.6 and Figure 6.7.

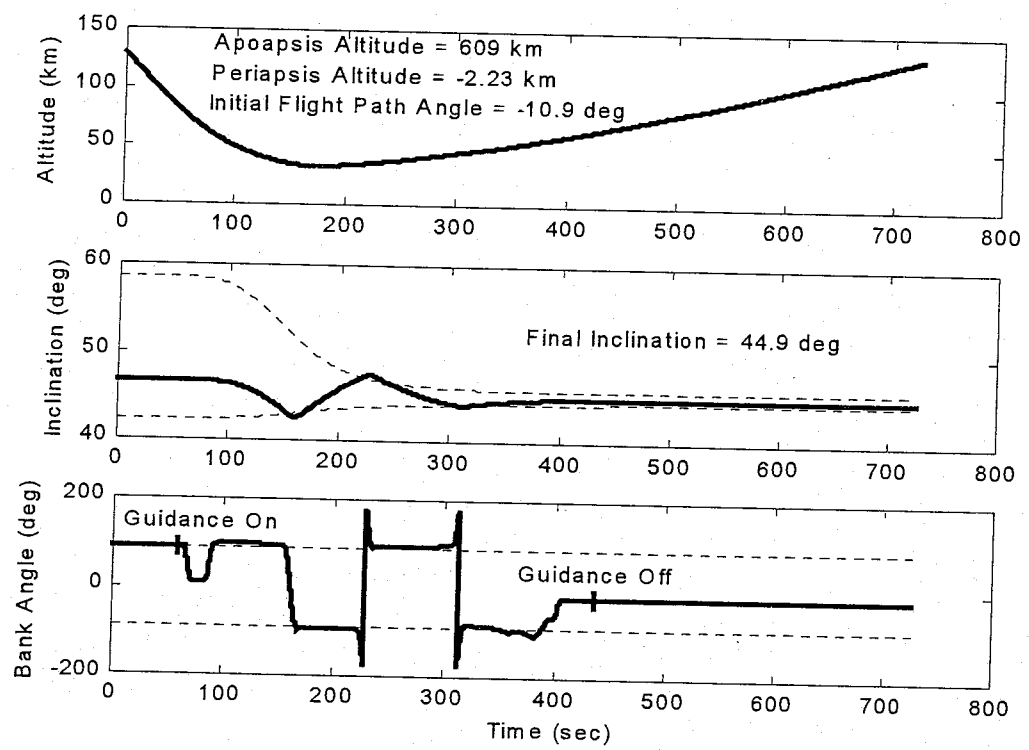


Figure 6.6: Full Simulation with +20 m/s Velocity Error

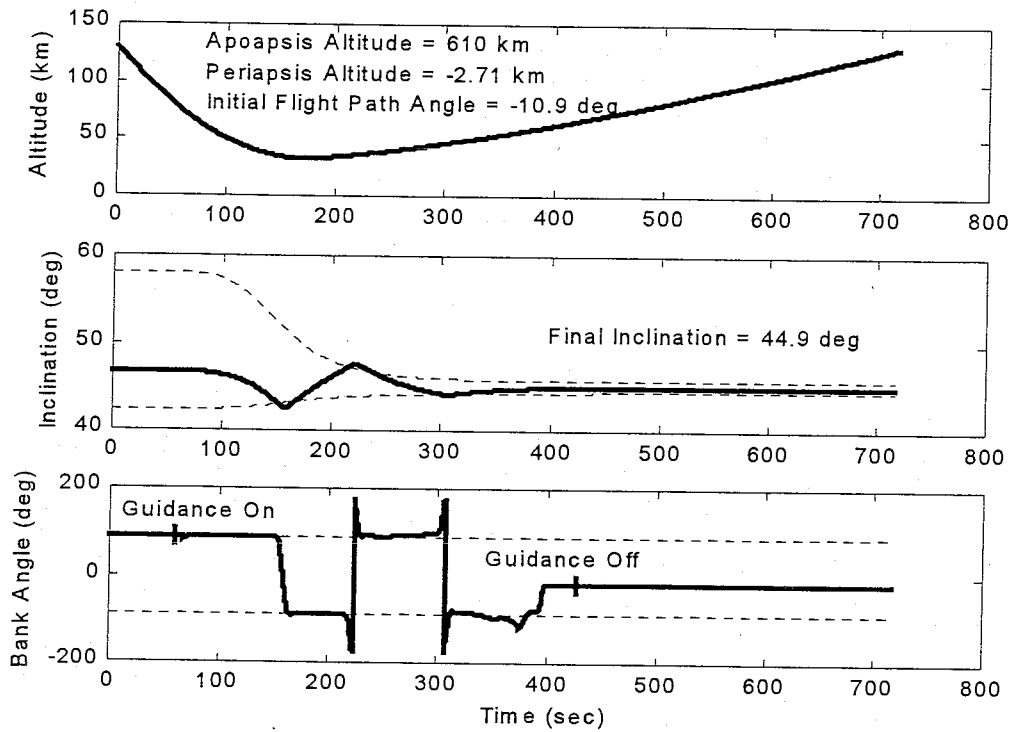


Figure 6.7: Full Simulation with -20 m/s Velocity Error

Both of these cases exhibit reasonable convergence to the desired exit state. All of the off nominal test cases presented thus far show that the guidance algorithm is capable of overcoming errors in the initial position and velocity of the vehicle.

Errors in the initial state are not the only errors likely to be encountered however. The atmospheric density at Mars is widely varying, and may deviate from mean conditions due to many kinds of conditions such as dust storms or weather conditions. To examine this possibility, slightly more and less dense Mars-GRAM atmospheric models were included to study the effects on the trajectory. The Mars-GRAM mean density previously used is an average of the atmospheric data contained in the model. For a less dense model, density values one standard deviation, or root-mean-square, less than the mean ($-1-\sigma$) were used. This is approximately a 16% variation from the mean at altitudes near the point of closest approach in this study. Similarly, the higher density model uses values one standard deviation greater than the mean ($+1-\sigma$). The variation is approximately 19% higher than the mean at the same altitudes. These results are provided in Figure 6.8 and Figure 6.9.

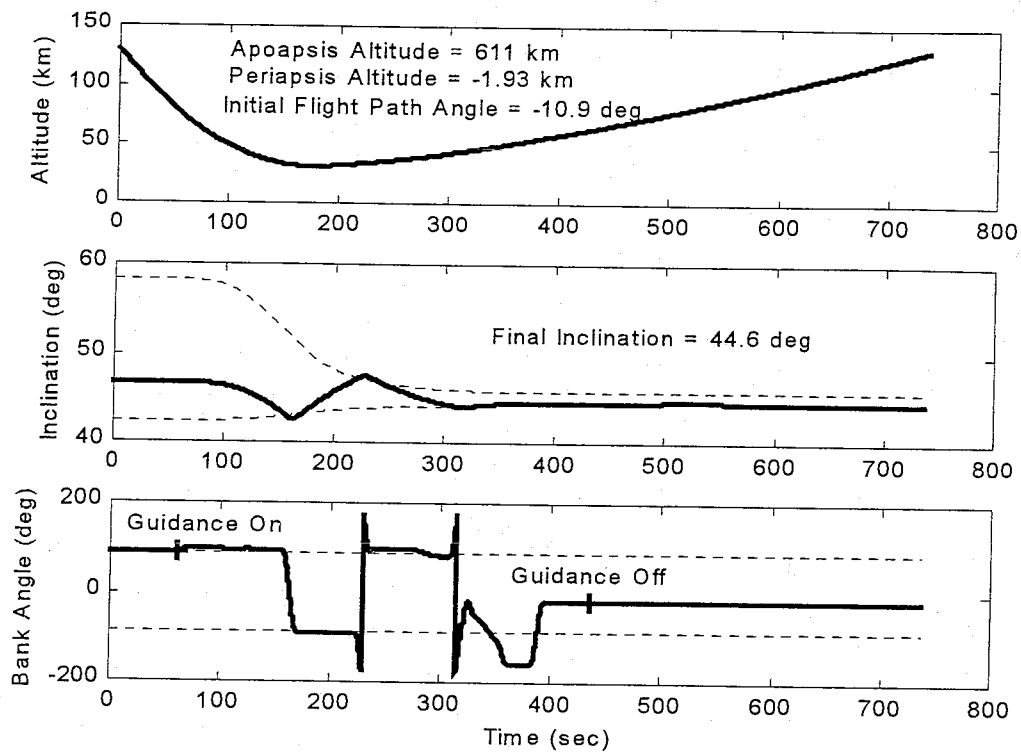


Figure 6.8: Full Simulation with Low Density Atmosphere

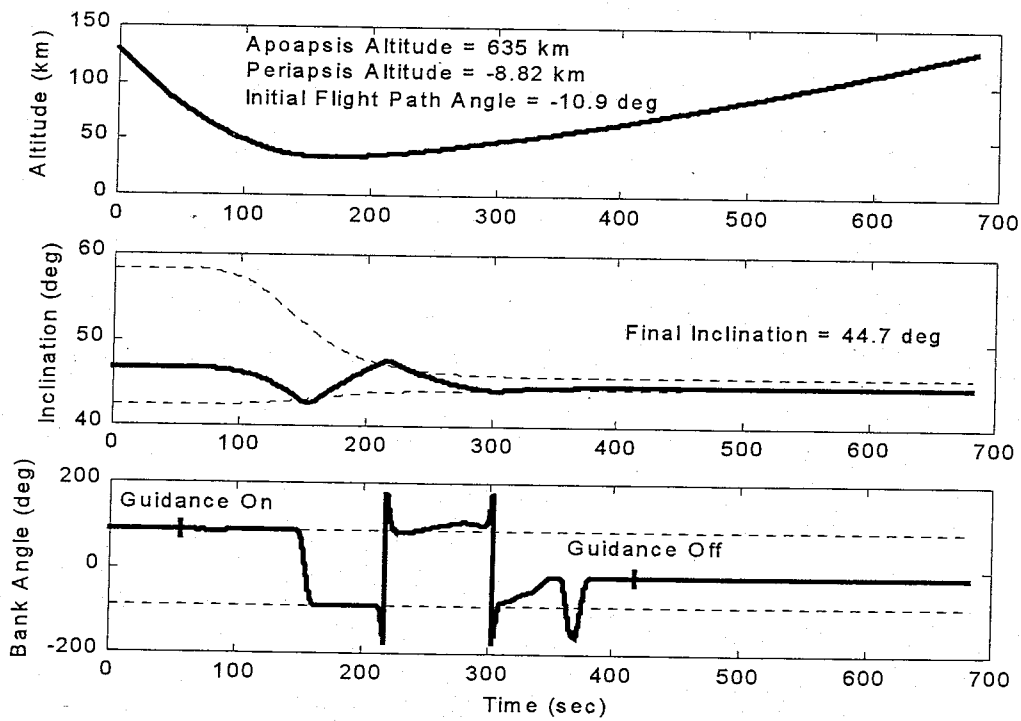


Figure 6.9: Full Simulation with High Density Atmosphere

Again, each of these simulations exhibited reasonable convergence to the target conditions. Unlike the two examples with flight path angle errors, deviations from the nominal trajectory are not immediately apparent. As the vehicle traverses through the atmosphere, the density variations cause gradual deviations from nominal. Therefore, small bank commands away from nominal are command for long durations all along the trajectory. These become more visible toward the end of the trajectory when commands become larger due to the decreased effectiveness in the upper atmosphere.

Another possible source of error are the vehicle characteristics themselves. Because of fuel usage, the mass of the vehicle at atmospheric entry is not precisely known. A source of greater error can be the aerodynamic coefficients. To simulate these possible errors, a $\pm 10\%$ deviation on the ballistic coefficient $\left(\frac{m}{C_D A}\right)$ and lift acceleration coefficient $\left(\frac{m}{C_L A}\right)$ was examined. The results of this study are presented in Figure 6.10 and Figure 6.11.

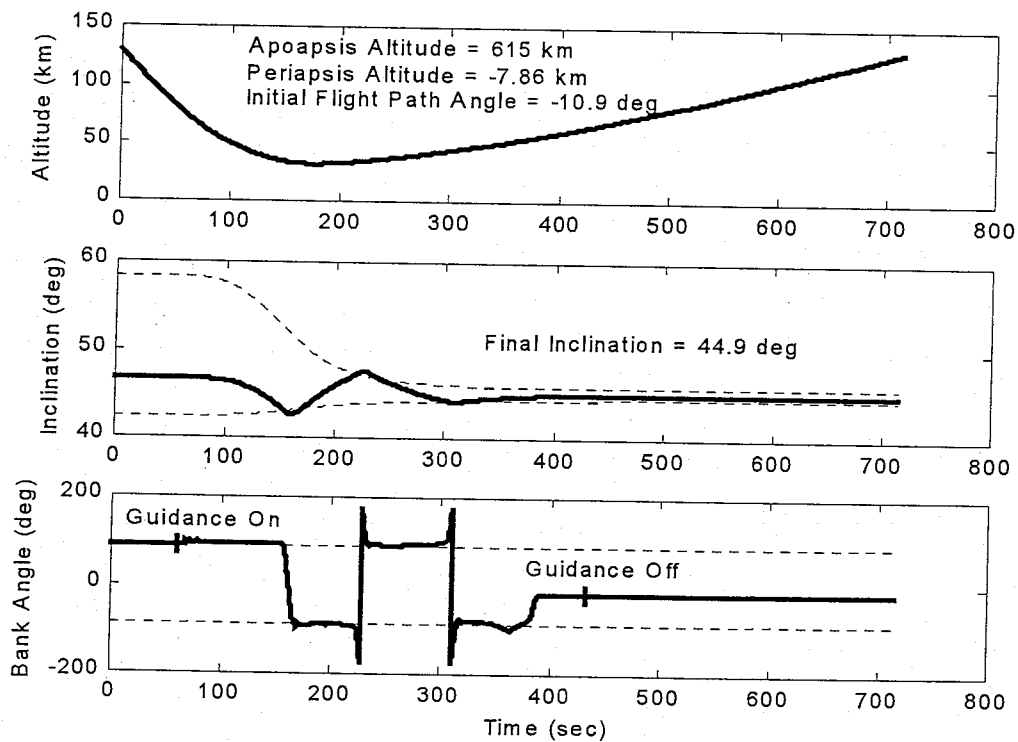


Figure 6.10: Full Simulation with +10% Ballistic Coefficient Error

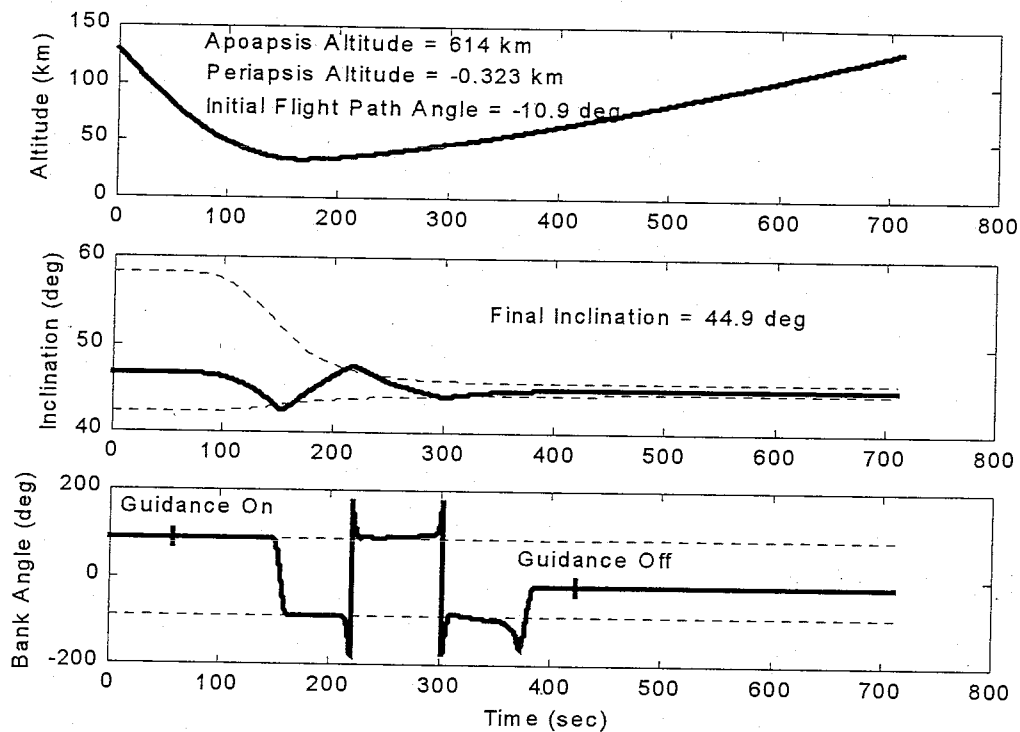


Figure 6.11: Full Simulation with -10% Ballistic Coefficient Error

Each of these test cases exits the atmosphere reasonably near the desired exit state. The test case results indicate that the robustness of the Apollo algorithm is not compromised by the addition of the bank direction control logic. The largest error in the final apoapsis altitude is only about 5.8% from the 600 km target for the cases studied. This indicates that the control law may be applicable to guidance routines and actual missions. Due to the high degree of non-linearity of this problem, however, it is possible that the combined affects of more than one of these errors occurring simultaneously would result in greater errors in the final state.

A summary of all of the full simulation results is presented in Table 6.1. An illustration of the results is provided in Figure 6.12.

Table 6.1: Summary of Full Simulation Test Cases

Test Case	Final Inclination Angle	Final Apoapsis Altitude	Final Periapsis Altitude
Nominal	44.9	609	-2.37
-0.5 deg Flight Path Angle	44.9	615	-5.24
+0.5 deg Flight Path Angle	44.9	597	3.43
+0.5 deg Azimuth Angle	44.9	609	-2.40
-0.5 deg Azimuth Angle	45.0	610	-2.44
+20 m/s Velocity	44.9	609	-2.23
-20 m/s Velocity	44.9	610	-2.71
Low Density Atmosphere	44.7	611	-1.93
High Density Atmosphere	44.6	635	-8.82
+10% Ballistic Coefficient	44.9	615	-7.86
-10% Ballistic Coefficient	44.9	614	-0.32

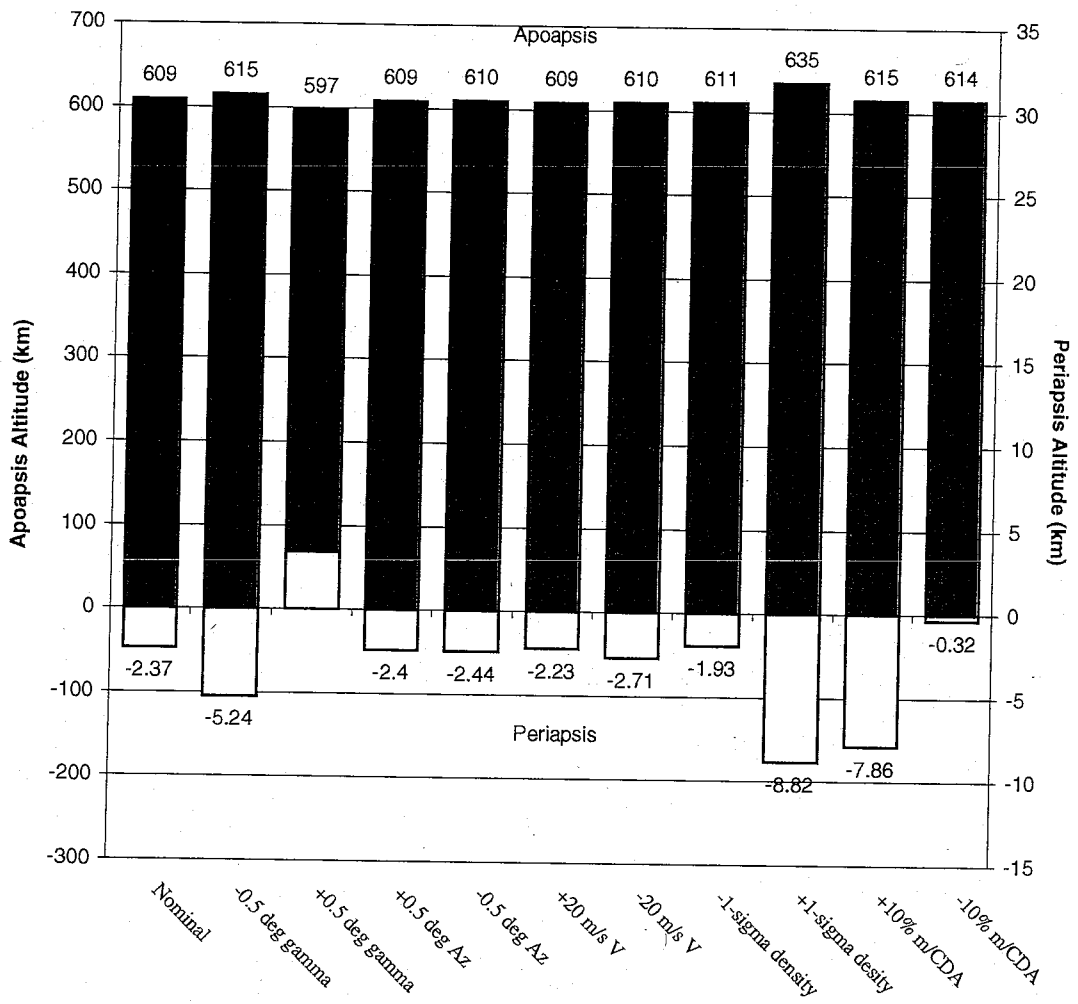


Figure 6.12: Results of Full Simulation Test Cases

7 Conclusions

A control law was developed to designate the bank direction for use in a bank reversal aerocapture guidance algorithm to maximize the periapsis altitude of the final orbit. In addition, a method for defining inclination boundaries for bank reversals was examined. Also, to generate a 3-DOF simulation that more closely approximates a 6-DOF simulation, an angular motion algorithm was created.

A trade study in which bank reversals were performed in different directions during various portions of the aerocapture trajectory showed that the periapsis was higher when a reversal conducted through lift up occurred in the first part of the trajectory and when a reversal conducted through lift down occurred in the later part of the trajectory. This trend was confirmed by examining the orbital equations. The theory proved that lift up accelerations increased the periapsis in the portion of the trajectory before the point of closest approach, and lift down accelerations produced the same results in the trajectory following the point of closest approach. Furthermore, a sensitivity analysis included in the simulations showed the affects of lift up or lift down accelerations on the periapsis agreed with the theory.

All of the findings came together to form a complete simulation including a bank reversal guidance algorithm. A series of varying scenarios were explored in both nominal trajectories and the complete simulation to confirm the control law. In general the expected behavior was observed in the periapsis histories. In some cases, however, the final periapsis altitude did not follow the expected trend. It was found that this represented the extreme sensitivity of the final periapsis to the initial flight path angle.

Various test cases were examined using the complete simulations. It was found that the control law could be integrated into a guidance algorithm without adversely affecting the reliability of that algorithm. The affect of small changes in the bank angle from nominal (held for relatively long times) on the final periapsis proved significant. This is a significant factor in the full simulation when bank angle changes are required for apoapsis targeting.

The control method applied in this study did increase the periapsis of the final orbit, but it did not result in an increase of more than a few tens of kilometers. It is believed this is due to selecting the 90 degree nominal bank angle. This constraint greatly reduces the potential for gains available from the control method. While it proved convenient for

studying the affect of the vertical component of lift on the periapsis altitude, it did not fully exploit the capabilities of the control method because only the brief bank reversals had any influence.

An alternative nominal trajectory was examined with a nominal bank angle chosen to produce vertical components of lift for increasing the periapsis altitude. It is believed there is potential for greater advantages by using a similar approach. This method was not fully explored in the study due to the sensitivity to initial conditions and other reasons aimed at concentrating on bank reversal affects only.

Overall, the control law developed shows that the final periapsis altitude following an aerocapture pass is increased by:

- (1) A positive vertical component of lift while descending (flight path angle is negative)
- (2) A negative vertical component of lift while ascending (flight path angle is positive)

8 Future Work

There is more that could be explored before realizing the full potential of exploiting what was discovered by the theory. The 90 degree nominal bank angle assumption, while valuable for this study, is not necessary for any actual application. There exists the likelihood of another nominal bank angle providing equally sufficient control authority while resulting in better results in terms of a higher periapsis.

It was discovered that the final periapsis altitude is extremely sensitive to a small vertical component of lift if it exists for a long duration. A scheme could be developed to design the nominal bank angle to increase the periapsis altitude at all times, not just during reversals. One such scenario was examined with encouraging results in terms of periapsis altitude. However, the sensitivity of the trajectory to off nominal conditions made it not applicable to this study. This method and other possible techniques do deserve future attention to realize gains such as those suggested here.

Additional modifications could be made to the Apollo algorithm to use more of the potential of these findings. Instead of allowing lift up commands to be issued near atmospheric exit, it is possible to force lift down commands for additional periapsis gain. Also, the inclination corridor could be modified to force a reversal early in the trajectory when the sensitivity magnitude is large. This method must consider that the amount of lift produced may be low due to low density at high altitudes. Trade studies could identify the best combination of high density and high sensitivity magnitude for maximum effectiveness.

It is also quite possible that an altogether original guidance algorithm could be developed using these discoveries. There is no reason that the nominal bank angle must be a constant other than simplicity. Prospective nominal trajectories can take on almost any form. It is almost certain that some exist with superior results if the theory is properly employed.

Additional trade studies could be performed to apply this control method to an aerobraking orbit. During each pass through the atmosphere, drag could be used to lower the apoapsis as usual, while lift could be used to increase the periapsis. This could be used to fly deeper into the atmosphere and reduce the adjustment ΔV required to set up for the next pass.

Other uses and advantages might be discovered if this method is applied to a 6-DOF simulation containing a RCS model.

References

1. Sheehan, William. The Planet Mars. A History of Observation and Discovery. The University of Arizona Press. 1996.
2. Braun, R. D., et. al. *Mars Pathfinder Atmospheric Entry Navigation Operations.* AIAA 97-3663. Reston, Va. 1997.
3. Shane, Russell W., Didier F. G. Rault, and Robert H. Tolson. *Mars Global Surveyor Aerodynamics for Maneuvers in Martian Atmosphere.* AIAA 97-2509. Reston, Va. 1997.
4. Powell, Richard W. *Numerical Roll Reversal Predictor-Corrector Aerocapture and Precision Landing Guidance Algorithms for the Mars Surveyor Program 2001 Missions.* AIAA 98-4574. Reston, Va. 1998.
5. Ro, T. and E. Queen. *Study of Martian Aerocapture Terminal Point Guidance.* AIAA 98-4571. Reston, Va. 1998.
6. Powell, R. W., et. al. Program to Optimize Simulated Trajectories (POST) – Volumes I and II. Formulation and Utilization Manuals. October 1997.
7. Striepe, Scott A., et. al. *An Atmospheric Guidance Algorithm Testbed for the Mars Surveyor Program 2001 Orbiter and Lander.* AIAA 98-4569. Reston, Va 1998.
8. Hoffman, Stephen J., David I. Kaplan, Editors. Human Exploration of Mars: The Reference Mission of the NASA Mars Exploration Study Team. NASA-SP 6107. July 1997.
9. Drake, Bret G., Editor. Reference Mission Version 3.0 Addendum to the Human Exploration of Mars: The Reference Mission of the NASA Mars Exploration Study Team. NASA EX13-98-036. June 1998.
10. Lebeau, Jay. Human Mission Architecture Support Aerodynamicist. NASA Johnson Space Center.
11. Vaughan, Robin. *Planetary Constants and Models.* Mars Pathfinder Project. JPL D-12947. December 1995.
12. Justus, C. G., B. F. James. Mars Global Reference Atmospheric Model (Mars-GRAM) Version 3.8: Users Guide. NASA-TM 209629. May 1999.
13. Bate, Roger R., Donald D. Mueller, and Jerry E. White. Fundamentals of Astrodynamics. Dover Publications, Inc. New York. 1971.

14. Battin, Richard H. An Introduction to The Mathematics and Methods of Astrodynamics. AIAA Education Series. New York. 1987.
15. Bryson, Arthur E. Jr., and Yu-Chi Ho. Applied Optimal Control. Hemisphere Publishing Corporation. New York. 1975.

Appendix A

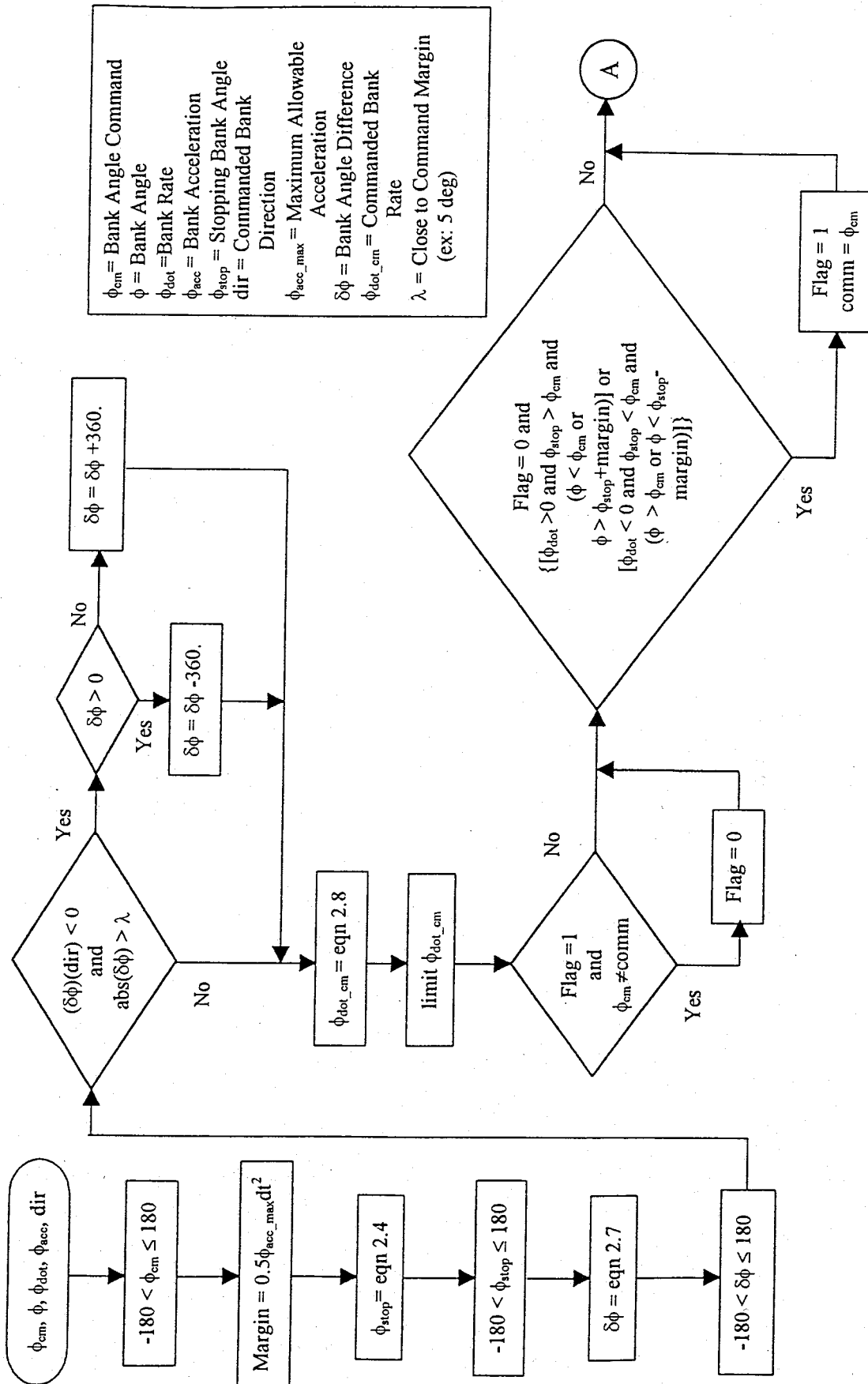


Figure A.1: Flow Chart of Bank Angle Dynamics Model

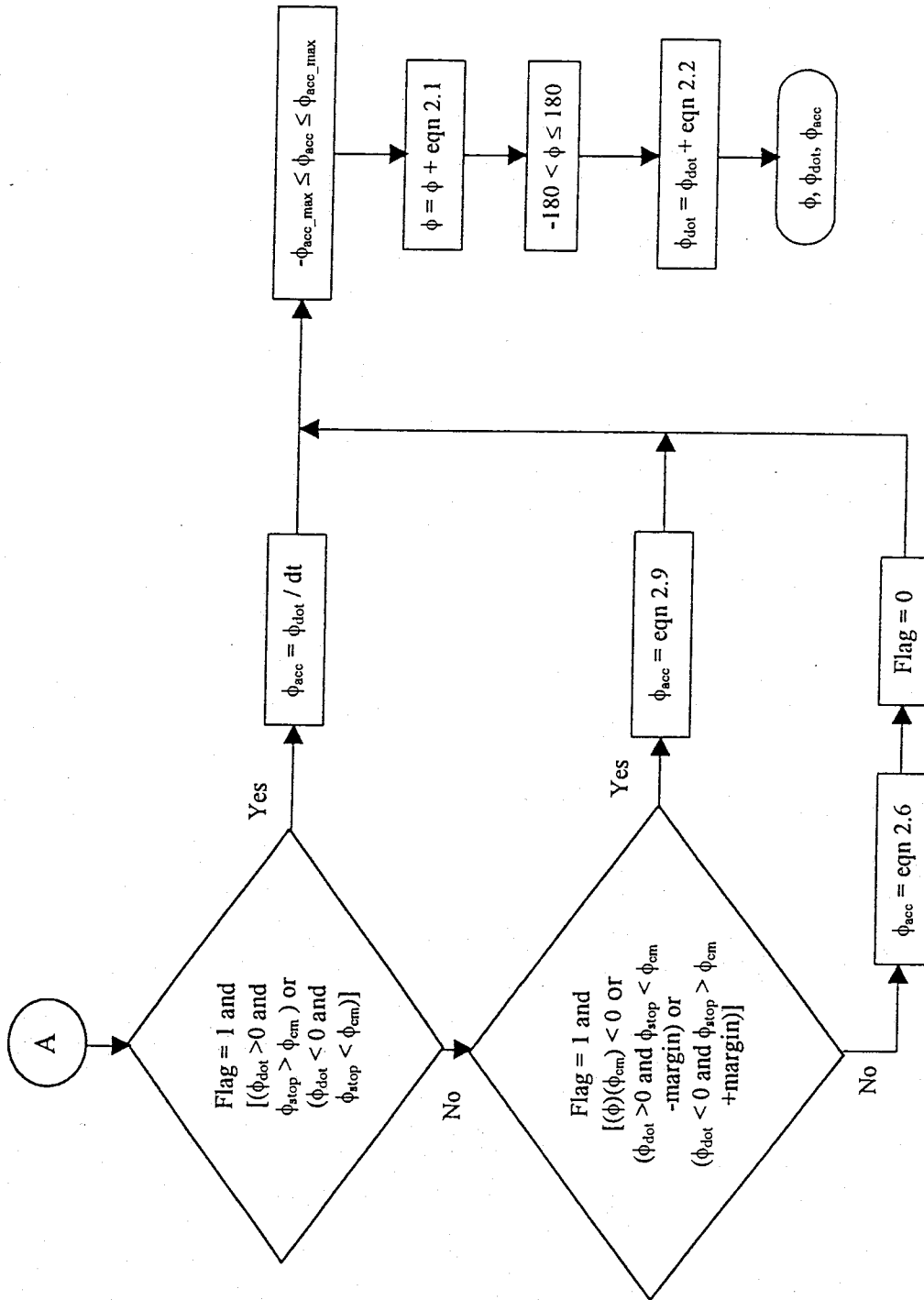
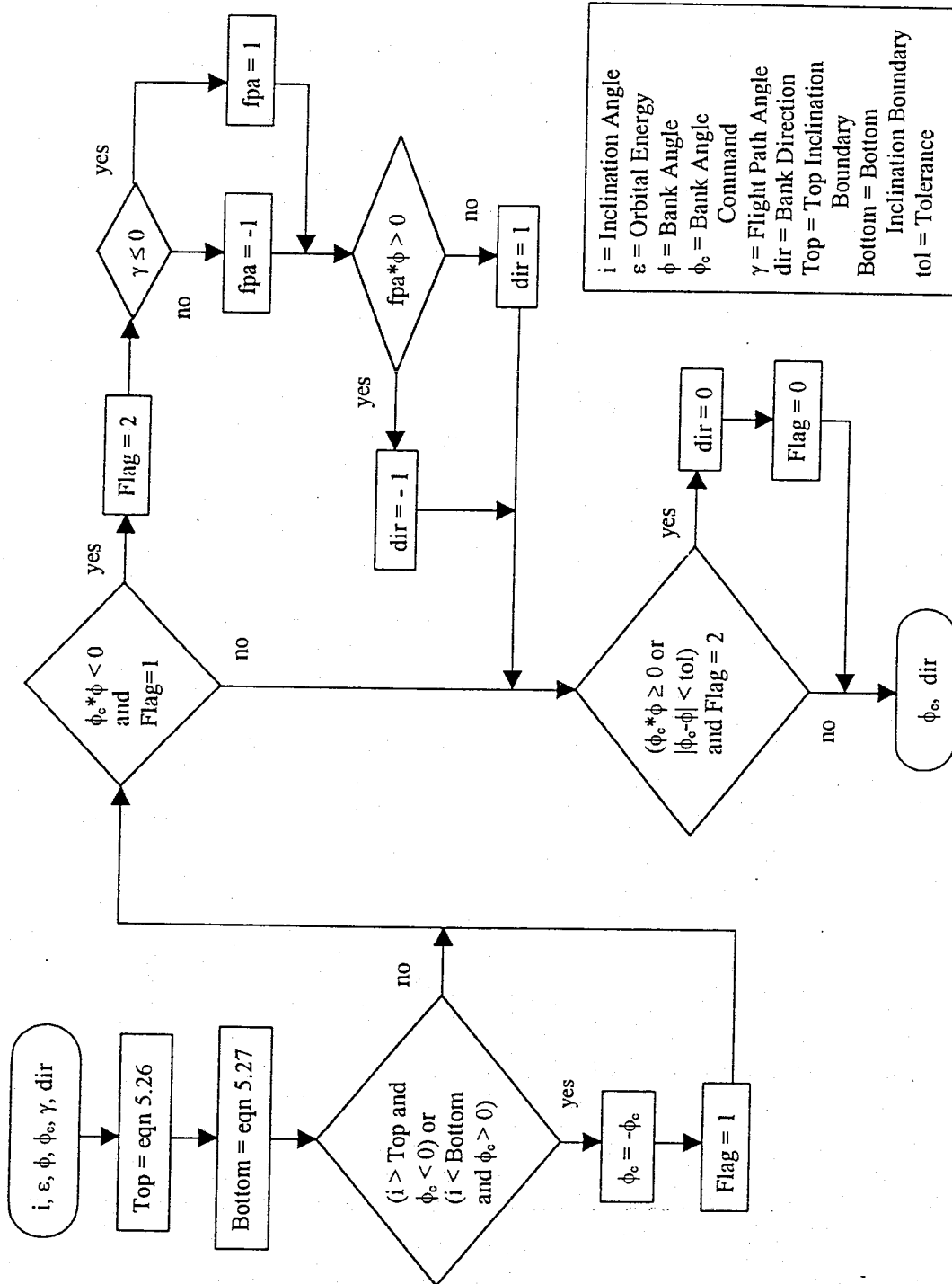


Figure A.2: Flow Chart of Bank Angle Dynamics Model (cont.)

Appendix B



i = Inclination Angle
 ϵ = Orbital Energy
 ϕ = Bank Angle
 ϕ_c = Bank Angle Command
 γ = Flight Path Angle
 dir = Bank Direction
 Top = Top Inclination Boundary
 Bottom = Bottom Inclination Boundary
 tol = Tolerance

Figure B.1: Flow Chart of Bank Reversal Control Logic